EVOLUTION
INTERNATIONAL JOURNAL OF ORGANIC EVOLUTION

Patterns of morphological integration in the appendicular skeleton of mammalian carnivores

Journal:	*Evolution*
Manuscript ID:	14-0525.R1
Manuscript Type:	Original Article
Date Submitted by the Author:	n/a
Complete List of Authors:	Martín-Serra, Alberto; Universidad de Málaga, Ecología y Geología Figueirido, Borja; Universidad de Málaga, Ecología y Geología P,rez-Claros, Juan; Universidad de Málaga, Ecología y Geología Palmqvist, Paul; Universidad de Málaga, Ecología y Geología
Keywords:	Appendicular skeleton, Carnivorans, Morphological integration, Locomotion, Cursorial, Morphometrics

Patterns of morphological integration in the appendicular skeleton of mammalian carnivores

Alberto Martín-Serra[1,2 *], Borja Figueirido[1,3], Juan Antonio Pérez-Claros[1,4] & Paul Palmqvist[1,5]

[1]Departamento de Ecología y Geología, Facultad de Ciencias, Universidad de Málaga, Campus de Teatinos s/n, 20971-Málaga, Spain. E-mail: [2]almarse@uma.es, [3]borja.figueirido@uma.es, [4]johnny@uma.es, [5]ppb@uma.es

Short-title for page headings: Integration in carnivoran appendicular skeleton

*Author for correspondence

Alberto Martín-Serra

Departamento de Ecología y Geología de la Facultad de Ciencias de la Universidad de Málaga, 29071-Málaga, Spain

E- mail: almarse@uma.es

Telephone: +34 952 13 16 65

ABSTRACT

We investigated patterns of evolutionary integration in the appendicular skeleton of mammalian carnivores. The findings are discussed in relation to performance selection in terms of organismal function as a potential mechanism underlying integration. Interspecific shape covariation was quantified by 2B-PLS analysis of 3D landmark data within a phylogenetic context. Specifically, we compared pairs of anatomically connected bones (within-limbs) and pairs of both serially homologous and functional equivalent bones (between-limbs). The statistical results of all the comparisons suggest that the carnivoran appendicular skeleton is highly integrated. Strikingly, the main shape covariation relates to bone robustness in all cases. A bootstrap test specifically developed to compare the degree of integration between specialized cursorial taxa (i.e., those whose forelimbs are primarily involved in locomotion) and non-cursorial species (i.e., those whose forelimbs are involved in more functions than their hind limb) showed that cursors have a more integrated appendicular skeleton than non-cursors. The findings demonstrate that natural selection can influence the pattern and degree of morphological integration by increasing the degree of bone shape covariation in parallel to ecological specialization.

KEYWORDS: Appendicular skeleton, carnivorans, morphological integration, locomotion, cursorial, morphometrics

INTRODUCTION

Integrated phenotypes that function as a whole are the result of interactions among their component parts (Olson and Miller 1951). The number and strength of these interactions have a strong effect on both trait variability and evolvability (e.g., see Olson and Miller 1951, 1958; Van Valen 1965; Cheverud 1996; Wagner and Altenberg 1996; Klingenberg and Zaklan 2000; Magwene 2001; Hansen 2003; Goswami 2006a; Young and Badyaev, 2006; Wagner et al. 2007; Hallgrímsson et al. 2009; Klingenberg 2010; Goswami and Polly 2010a, 2010b; Kelly and Sears 2011; Bennett and Goswami 2011; Bell et al. 2011; Chamero et al. 2013; Fabre et al. 2014; Goswami et al. 2014), and are also related to different developmental and evolutionary constraints (Cheverud, 1982, 1996; Wagner, 1996; Wagner and Altenberg, 1996; Arthur, 2001; Klingenberg, 2008; Futuyma, 2010). The nature of these interactions differs according to the type (or degree) of integration, because a given phenotype can be developmentally, genetically, functionally, or evolutionarily integrated (e.g., see Wagner 1996; Wagner and Altenberg 1996; Cheverud 1996; Hall 1999; Mezey et al. 2000; Monteiro et al. 2005; Breuker et al. 2006; Klingenberg 2008; Goswami 2006a, 2006b; Bell et al. 2011; Chamero et al. 2013; Figueirido et al. 2013; Klingenberg 2013; Fabre et al. 2014). However, phenotypic integration is a pervasive characteristic of organisms (Goswami et al. 2014) and although morphological integration and modularity are observed in covariations among multiple traits, the underlying mechanisms responsible for such integration are not usually observable. For this reason, the type of integration can be inferred from the covariation of morphometric variables, and hypotheses on the effects of these mechanisms can then be tested (Klingenberg 2013).

The pattern of morphological integration in the appendicular skeleton of mammals is of special interest given the singular hierarchical structure of the

interactions among the appendicular bones (*sensu* Hallgrímsson et al. 2002; Young and Hallgrímsson 2005). Limbs are serial homologues, as they have the same developmental origin (e.g., see Tickle 2002; Hallgrímsson et al. 2002; Young and Hallgrímsson 2005; Bininda-Emonds et al. 2007; Schmidt and Fischer 2009; Kelly and Sears 2011; Bennett and Goswami 2011; Bell et al. 2011). Given their shared developmental processes, there is a clear correspondence between girdles (scapula-pelvis), stylopods (humerus-femur), zeugopods (radius-tibia and ulna-fibula), and autopods (manus-pes). Furthermore, it has been hypothesized that a strong integration between the fore- and hind limb is the ancestral condition of all tetrapods (e.g., Young and Hallgrímsson 2005; Schmidt and Fischer 2009). However, integration between serially homologous elements can be modified to match the functional demands of a given structure (Cheverud 1996; Wagner and Altenberg 1996; Young and Hallgrímsson 2005; Lawler 2008; Schmidt and Fischer 2009; Bennett and Goswami 2011; Kelly and Sears 2011; Bell et al. 2011). For example, extreme functional divergence between the fore- and hind limb can modify the developmental integration of their serially homologous elements. This is the case of flying vertebrates such as bats, birds, and pterosaurs (Young and Hallgrímsson 2005; Bell et al. 2011) or marsupial (metatherian) mammals. Such modification occurs in the latter group because their reproductive strategy promotes divergence between both limbs due to the need for a forelimb climbing function in the altricial neonate (Sears 2004; Weisbecker et al. 2008; Goswami et al. 2009; Kelly and Sears 2010; Bennett and Goswami 2011; Geiger et al. 2014). In contrast, the limbs of generalized quadrupedal mammals tend to be highly integrated (Young and Hallgrímsson 2005; Schmidt and Fischer 2009; Bennett and Goswami 2011; Kelly and Sears 2011) as there is little functional divergence between them. However, some authors have proposed a clear dissociation between functionally equivalent elements and serial homologues in

quadrupedal mammals (Raich and Casinos 1991; Gasc 2001; Schmidt and Fischer 2009). The reason underlying this proposal is that the reduction of the clavicle in several mammalian lineages (Polly 2007) allows the scapula to move more freely in the parasagittal plane (Jenkins 1974). As a consequence, the scapula contributes to stride length like the other major limb bones (Gasc 2001; Schmidt and Fischer 2009). Thus, the femur functions as the first element of the hind limb, while the scapula is its functional equivalent in the forelimb of mammals. Similarly, the humerus and the tibia function as the second element (Gasc 2001; Schmidt and Fischer 2009). As a consequence, the functional relationships among the bones of both limbs are decoupled from what is expected according to serial homology. Similarly, the fibula is largely reduced in mammalian carnivores (Polly 2007) and the tibia could have acquired some of its original functions, thus leading to functional convergence between the tibia and ulna.

The appendicular skeleton is an ideal system to study morphological integration because its functional and developmental units are incongruent (Fig. 1): although within-limb bones have distinct developmental origins, they contribute jointly to the same functions (Breuker et al. 2006). Therefore, by studying patterns of morphological integration in the appendicular skeleton we have the opportunity to test whether developmental processes have evolved to match the function of limb elements (i.e., the matching hypothesis of Wagner and Altenberg [1996]). Strikingly, in a recent paper on morphological integration and modularity, Klingenberg (2014) remarks the necessity of empirical studies testing the “matching hypothesis”.

In this article, we investigate the pattern and degree of morphological integration in the appendicular skeleton of mammalian carnivores (Mammalia; Carnivora) using pairs of serially homologous bones (i.e., scapula-pelvis, humerus-femur, radius-tibia)

and functionally equivalent bones (i.e., scapula-femur, humerus-tibia, ulna-tibia) (Fig. 1A). We also quantify integration between bones anatomically connected within limbs (Fig. 1A), which interact functionally (e.g., see Fabre et al. 2014). Our main objective is to test whether developmental processes have evolved to match the functional structure of the locomotion system, which will allow to better understand the "matching hypothesis" of Wagner and Altenberg (1996).

We used mammalian carnivores as a case study because they are a notable exception among quadrupeds in that they show a substantial functional divergence between both limbs. In fact, whereas the carnivoran hind limbs are only involved in moving the animal forward, the forelimbs are usually adapted to different functions such as manipulating objects in the case of omnivores/herbivores or grappling with prey in the case of predators (Gonyea 1978; Van Valkenburgh 1985; Van Valkenburgh 1987; Iwaniuk and Wishaw 1999, 2000; Iwaniuk et al. 1999, 2000; Andersson 2003, 2004, 2005; Schutz and Guralnick 2007; Walsmley et al. 2011; Meloro et al. 2013; Samuels et al. 2013; Fabre et al. 2013). Strikingly, several taxa have secondarily lost most of the forelimb skills not directly related to terrestrial locomotion (e.g., the more specialized cursorial taxa). This is because there is a functional conflict between an efficient terrestrial locomotion (Janis and Wilhelm 1993) and the ability to manipulate items with the forelimbs (Andersson 2004; Andersson and Werdelin 2003; Figueirido and Janis 2011; Janis and Figueirido 2014). Efficiency of locomotion is fostered by having a specialized forelimb with the range of motion of the elbow joint restricted to the parasagittal plane. However, this also precludes forearm supination, which is essential for developing additional forelimb skills (e.g., see Andersson and Werdelin 2003; Schutz and Guralnick 2007; Figueirido and Janis 2011; Janis and Figueirido 2014). Thus, we compared the degree of bone shape covariation between cursorial and non-

cursorial carnivorans to explore the effects of functional specialization on the patterns of morphological integration in the appendicular skeleton of mammalian carnivores. However, it is worth noting that several studies have provided different definitions of the term cursorial. For example, Hildebrand (1985) defined cursors as "quadrupeds that commonly run and are structurally modified to benefit speed or endurance". Taylor (1989) identified three types of cursors: (1) those that are capable of low-speed prolonged trotting (e.g., hyaenids and most canids); (2) those that run fast and depend on both speed and stamina (e.g., wolves); and (3) those that are sprinters, capable of very rapid acceleration (e.g., the cheetah, *Acinonyx jubatus*). Alternatively, Samuels et al. (2013) considered as cursorial carnivorans only those taxa that "regularly display rapid locomotion with bounding characterized by unsupported intervals."

In any case, we use the term cursor in a broader sense, by including in this category all carnivorans whose forelimbs are used primarily for terrestrial locomotion (i.e., many canids, hyaenids, and the cheetah among felids; see Table 1 for references), whereas the non-cursor category includes: *(i)* ambushing carnivorans that grapple with prey (i.e., all felids except the cheetah; see Table 1); *(ii)* species with digging, climbing or swimming abilities (e.g., the European badger, the raccoon or the northern river otter; see Table 1), in which the fore- and hind limbs have different functions during these activities; and *(iii)* species that usually manipulate items with their forelimbs (i.e., most mustelids, procyonids, ursids and ailurids; see Table 1). It is worth noting that some canids with climbing or swimming abilities have also been classified as non-cursors (i.e., grey fox, bush dog and raccoon dog; see Table1), as these activities could imply functional differences between limbs. In contrast, the fully terrestrial maned wolf (Kleiman 1972; Dietz 1985) has been classified as cursor (unlike Samuels et al. 2013). The reason is that this species behaves in a similar fashion to any other fox and does not

manipulate items nor grapples with prey (Langguth 1975; Bestelmeyer and Westbrook 1998; Rodden et al. 2004), using the forelimb primarily for terrestrial locomotion.

We hypothesize that the appendicular skeleton of carnivorans is highly integrated at an evolutionary level. However, we predict that both developmental and functional interactions are potential sources of within- and between-limb integration. Furthermore, we hypothesize that the increased functional association between both limbs in cursorial taxa has generated, by performance selection, a more integrated appendicular skeleton in this group of carnivorous mammals (see Fig. 1B).

MATERIAL AND METHODS

Data

The data set comprised the following appendicular bones: scapula, humerus, radius, ulna, pelvis, femur, and tibia from 46 living species (Table 1). It is worth noting that only one side of the pelvic girdle (the innominate bone) was analysed. Although special attention was paid to families with large representatives (e.g. felids, canids, hyaenids, and ursids), several species of mustelids, procyonids, and ailurids were also included to cover a wider range of carnivoran ecomorphological diversity. As indicated by complete epiphyseal fusion to diaphysis, only adult specimens were collected to avoid the effects of ontogenetic variation. Furthermore, only bones from the same side of an individual were collected to avoid the effects of left-right asymmetry. All the specimens analysed (Table S1) were housed at the American Museum of Natural History (AMNH, New York) and the Natural History Museum (NHM, London).

Geometric morphometrics

A set of 3D homologous landmarks was directly digitized onto each bone using a Microscribe G2X digitizer. The landmarks (Fig. 2) were selected according to different anatomical criteria (Table S2). The 3D coordinates (x,y,z) of all the landmarks were

imported into *Excel* using the Immersion software package (Immersion, Inc). The surface of each appendicular bone of a jaguar (*Panthera onca* [AMNH-139959]) and the pelvis of a snow leopard (*Uncia uncia* [AMNH-100110]) housed at the American Museum of Natural History (Mammalogy Department) were scanned using a 3D-mobile surface scanner (Nextengine HD) and the *ScanStudio Pro I* software package. Our aim was to locate the landmarks digitized onto the sample specimens in the 3D models in order to transform them into each of the models derived from statistical analyses using a morphing procedure (Wiley et al. 2005; Drake and Klingenberg 2010; Schoenebeck et al. 2012; Singleton 2012; Martín-Serra et al. 2014a). The morphing procedure was performed with the *Landmark* software package from the Institute of Data Analysis and Visualization (IDAV 2002-2006).

A Procrustes fit (Dryden and Mardia 1998) was individually performed on the raw coordinates of the landmarks digitized on each bone using the *MorphoJ* software package (Klingenberg 2011), which removes the effects of rotation, translation, and scaling (Rohlf and Marcus 1993). Once the specimens were aligned, Procrustes coordinates and centroid size were both averaged by species. We analysed species averages instead of specimens for the following reasons: *(i)* our main aim was to study the influence of functional adaptations in the patterns of morphological integration at an evolutionary level; for this purpose, interspecific covariation patterns are more likely to reflect these effects than intraspecific ones, which may also reflect developmental constraints in the appendicular skeleton (Klingenberg 2008); *(ii)* furthermore, it is more appropriate to analyse species averages than specimens in order to avoid mixing the effects of intra- and interspecific covariation and allometry (e.g., see Fabre et al. 2014); and *(iii)* the independent contrasts used to correct for phylogenetic effects on the patterns of covariation were performed using species averages.

226 ***Accounting for the effects of size and phylogeny***

227 We investigated the effects of both size and phylogeny on bone shape variation given
228 that they can influence the degree of covariation between pairs of morphological
229 structures.

230 A phylogenetic tree was assembled (Fig. 3) using the *Mesquite* software package
231 (Maddison and Maddison, 2011) to test for the presence of a phylogenetic signal in the
232 sample. The tree was based on the topology and branch lengths (million years before
233 present) of previously published phylogenies (Koepfli et al. 2007; Nyakatura and
234 Bininda-Emonds 2012). The tree topology was based on the phylogeny proposed by
235 Nyakatura and Bininda-Emonds (2012). However, the well-developed phylogeny
236 created by Koepfli et al. (2007) for the family Procyonidae was used to avoid
237 polytomies.

238 ,A multivariate regression (Monteiro 1999) of Procrustes coordinates on centroid
239 size was performed in each bone to investigate the influence of size on bone shape. A
240 permutation test (10,000 permutations) was used to assess the statistical significance of
241 all regressions (Drake and Klingenberg 2008). The shape of those bones that showed
242 significant interspecific allometry was decomposed into residual and predicted
243 components (Drake and Klingenberg 2008). These residuals were used in subsequent
244 multivariate analyses to explore the morphological covariation that accounts for size
245 effects (hereafter called size-free species averages data).

246 The *MorphoJ* software package (Klingenberg 2011) was used to perform a
247 permutation test developed for multivariate analyses (Klingenberg and Gidaszewski
248 2010) to quantify the presence of phylogenetic signals in limb bone shape (Laurin
249 2004). This test compares the tree length calculated from shape data with the length of
250 10,000 random trees generated by permutations of the mean species shapes to the tips of

the phylogenetic tree. The *P*-value obtained indicates the proportion of trees that result in a tree length equal to or less than the reference tree and also indicates the statistical significance of the phylogenetic signal (Gidaszewski et al. 2009, Klingenberg and Gidaszewski 2010).

These analyses provided a new dataset derived from the phylogenetic independent contrasts of the PC scores (Felsenstein 1985), hereafter called size-free independent contrast data. We performed the independent contrast on the PC scores of all PCs because, while these are independent variables, Procrustes coordinates are intercorrelated and remove the same phylogenetic variance multiple times when they are used for independent contrast (P.D. Polly, pers. comm.). The phylogenetic signal of bone shape was also calculated on the PC scores instead of on the size-free species averages data for the same reason exposed above.

The standard deviations of the standardized contrasts were also obtained using the *Mesquite* software package (Maddison and Maddison 2011), allowing us to perform a multivariate regression (Monteiro 1999) of the contrasted PCs (through the origin) versus the standard deviations of the contrasts for each bone (following Díaz-Uriarte and Garland 1998). These regressions were performed with *MorphoJ* to determine whether there was a correlation between the contrasts of shape in relation to its standard deviations. A lack of correlation would indicate that the data satisfied the assumptions required by phylogenetic independent contrasts (Díaz-Uriarte and Garland 1998).

Covariation study

Covariation between bones was evaluated using two-block partial least-squares (2B-PLS) analysis (Rohlf and Corti 2000), which is a multivariate method used to calculate covariation between two blocks of variables that are treated symmetrically without assuming a causal relationship (Zelditch et al. 2004). Specifically, it is used to calculate

276 the linear combinations of the original variables (i.e., PLS or singular axes) that
277 maximize covariance between the two blocks (Rohlf and Corti 2000, Zelditch et al.
278 2004).

279 The degree of covariation between each pair of bone shapes was quantified
280 using the RV coefficient described by Escoufier (1973), extended in the context of
281 morphological integration and modularity by Klingenberg (2009), and applied to
282 morphometrics by several authors (e.g., see Goswami and Polly 2010b; Figueirido et al.
283 2013; Klingenberg and Marugán-Lobón 2013; Piras et al. 2013; Chamero et al. 2013;
284 Fabre et al. 2014; Goswami et al. 2014). This coefficient measures the degree of
285 covariation between two blocks of variables in relation to the total amount of variance
286 of each block (Klingenberg 2009) and is calculated as:

287 $$\mathrm{RV} = tr(S_{12}S_{21})/[tr(S_1S_1)tr(S_2S_2)]^{1/2}$$

288 where *tr* is the trace (i.e., the sum of the diagonal elements of a squared matrix),
289 S_{12} is the matrix of covariance between the two blocks (S_{21} is the transpose), and S_1 and
290 S_2 are the matrices of covariance within each of the two blocks, respectively
291 (Klingenberg 2009).

292 A permutation test with 10,000 permutations was performed to assess the
293 statistical significance of this coefficient against the null hypothesis of the complete
294 absence of covariation between the two blocks of variables. This test randomly shuffles
295 the observations of the subsets and re-calculates the RV coefficients. The proportion of
296 random RV coefficients equal to or higher than the actual RV coefficient yields a *P*-
297 value that indicates the presence of statistically significant covariation. The *MorphoJ*
298 software package (Klingenberg 2011) was used to perform these analyses.

299 We used 2B-PLS analyses and the RV coefficient to study the degree of
300 covariation between pairs of bones within limbs and between limbs (Fig. 1A). The

301 analysis of within-limbs covariation was restricted to comparisons of anatomically
302 connected bones, leading to a total of six pairs: four for the forelimb (i.e., scapula-
303 humerus, humerus-radius, humerus-ulna, and radius-ulna) and two for the hind limb
304 (pelvis-femur, femur-tibia). Within-limb integration was used as a "control" for
305 comparison with the between-limbs integration patterns. Between-limbs covariation was
306 analyzed by comparing pairs of serially homologous bones and functionally equivalent
307 bones in the fore- and hind limb. In the case of serially homologous bones, girdles
308 (scapula-pelvis), both stylopods (humerus-femur), and two zeugopods (radius-tibia)
309 were compared. The fibula was not included in the analysis because of its small size in
310 carnivorans and thus the ulna-fibula comparison was not considered in the serial
311 homology analysis. In line with Raich and Casinos (1991), Gasc (2001) and Schmidt
312 and Fischer (2009), three pairs of functionally equivalent bones were also compared:
313 ulna-tibia, scapula-femur, and humerus-tibia.
314 The set of 2B- PLS analyses and the RV coefficients were calculated using three
315 different datasets: *(i)* from the average of the Procrustes coordinates by species, to
316 explore shape covariation without accounting for the effects of phylogeny and size; *(ii)*
317 from the size-free species average data (i.e., residuals that only account for interspecific
318 allometry); and *(iii)* from the size-free independent contrast data (i.e., PCs that account
319 for both interspecifc allometry and phylogenetic relationships). The previous section
320 provides a detailed explanation of how these datasets were obtained.
321 An angular comparison between the respective PLS axes (Cheverud 1982;
322 Klingenberg and Zimmermann 1992; Klingenberg and McIntyre 1998; Klingenberg and
323 Zaklan 2000) was performed to test whether the main morphological changes that
324 associate a given bone with each of the other bones are the same. Angular comparison
325 was used to calculate the angle between the directions of two vectors – in our case, two

PLS axes – and to compare them to the distribution of angles obtained by simulating 100,000 random vectors within an *n*-dimensional morphospace (*n* depends on the number of landmarks). The proportion of angles equal to or less than the one obtained for the actual vectors indicates the *P* value, which shows whether the shape changes explained by one PLS axis are statistically different from those explained by other axes (e.g., it shows whether the first PLS axis obtained for the radius in the humerus-radius comparison is similar to the one obtained in the radius-ulna comparison). The *MorphoJ* software package (Klingenberg 2011) was used for the PLS and angular comparisons.

Testing the influence of functional specialization on limb bone integration

The effect of functional specialization on the patterns of covariation in the appendicular skeleton of carnivorans was explored by classifying the species into two functional categories: cursors and non-cursors (Table 1). Species with a functional similarity in their fore- and hind limbs during locomotion were classified as cursors and species with forelimbs with more functions than their hind limb, thus having a functional dissociation between both limbs, were classified as non-cursors (see Introduction).

A bootstrapping approach was used to test differences in RV coefficients between both ecological groups for all pairs of bones (i.e., comparisons within limbs, and between serially homologous and functionally equivalent bones) in order to investigate whether the limb bones of cursors and non-cursors have different degrees of morphological integration. Given that the RV coefficient is directly comparable to a squared correlation coefficient (Klingenberg 2009; Josse et al. 2008), confidence intervals were obtained for the differences between any pairs of RV coefficients using the procedure developed by Chan (2009) for squared multiple correlation coefficients. The bootstrap samples were generated by randomly drawing N1 and N2 observations with replacement from cursors and non-cursors, respectively. In each step, differences

were calculated between the RV coefficients for cursors and non-cursors. Obviously, differences close to zero suggest similarity in the RV coefficients of both groups. Using a sample of 10,000 differences, 90% and 95% bootstrap standard confidence intervals and bootstrap percentile intervals were constructed. The null hypothesis of equality between the two population RV coefficients was rejected if the zero value was outside these intervals (see Manly 2007: p. 62). The *Mathematica* software package (Wolfram, 2005) was used to perform the bootstrapping procedures.

Different Procrustes alignments for each functional subsample were calculated and the influence of size and phylogeny was again tested for each individual subsample. Similarly, the 2B-PLS analyses were performed and their respective RV coefficients were also calculated for both subsamples independently, using the size-free species averages data and the size-free independent contrast data.

RESULTS

Influence of body size and phylogeny on the shape of appendicular bones

Effects of interspecific allometry were significant for all bones in the whole sample, with the only exception of the tibia (Table 2). Furthermore, the phylogenetic signal in shape (PC scores) was statistically significant for all bones (Table 2). The regressions between the contrasts of shape on their respective standard deviations were not significant (all *P*-values > 0.1). Therefore, the data satisfy the assumptions required for phylogenetic independent contrasts.

Patterns of limb covariation

(i) Covariation of bones within limbs

The RV coefficients obtained from all comparisons of bones within both limbs were highly significant ($P < 0.01$). The RV coefficients obtained with the Procrustes coordinates (Fig. 4A, *left*) and the size-free coordinates for the species averages (Fig.

376 4B, *left*) were higher than those obtained with the size-free independent contrasts (Fig.
377 4C, *left*). Furthermore, forelimb bones had a greater degree of covariance than hind
378 limb bones and this difference increased when allometric and phylogenetic effects were
379 taken into account (Fig. 4A-C; *left column*). Another important aspect of the integration
380 patterns of the appendicular skeleton was that covariance between long bones was
381 greater than between long and girdle bones of both limbs (Fig. 4A-C; *left column*).
382 Similarly, the percentages of covariance explained by the first PLS axes were
383 slightly lower in all comparisons when the size-free independent contrasts were used
384 (Table 3). In addition, these percentages were also lower for the girdle bones compared
385 to the percentages obtained for the long bones (Table 3). Figure 5 shows the scatter
386 plots of the first PLS axes of both blocks of variables and their associated
387 morphological changes obtained from the analyses performed with the size-free species
388 averages. The morphological change associated with these PLS axes was the degree of
389 robustness in all bone comparisons (Fig. 5A-D, F), except for the pelvis in the case of
390 the pelvis-femur comparison (Fig. 5E). In fact, as the femur becomes more robust, the
391 pelvis develops a narrower iliac crest and both the ischium and the pubic symphysis
392 become shorter (Fig. 5E).
393 The distribution of taxa along all the PLS axes is very similar: most living canids
394 (especially the maned wolf, *Chrysocyon brachyurus*) and some felids such as the
395 cheetah (*Acinonyx jubatus*), the bobcat (*Lynx rufus*), and the serval (*Leptailurus serval*)
396 occupy the morphospace region that corresponds to slender bones (Fig. 5A-F). In
397 contrast, the morphospace region for robust bones is occupied by species such as the
398 Northern river otter (*Lontra canadensis*), the European badger (*Meles meles*), the giant
399 panda (*Ailuropoda melanoleuca*), and the sloth bear (*Melursus ursinus*) (Fig. 5A-F).
400 The only exception to this pattern is that the scapula of ursids is extremely robust – and

401 that of felids is only moderately robust – in relation to the humerus, which leads to a
402 slightly different distribution of taxa in the scapula-humerus comparison (see Fig. 5A).
403 (ii) Covariation of bones between serial homologues
404 All the RV coefficients obtained from the comparisons of serially homologous
405 appendicular elements (i.e., girdles, stylopods, and zeugopods) were statistically
406 significant ($P < 0.01$). Similar to the case of the within-limb analyses, the RV
407 coefficients and the percentages of covariance explained by the first PLS axes (Table 3)
408 obtained from the Procrustes coordinates (Fig. 4A, *centre*) and the size-free species
409 averages (Fig. 4B, *centre*) were higher than those obtained with the size-free
410 independent contrasts (Fig. 4C, *centre*). Furthermore, the RV coefficients obtained from
411 each comparison gradually increase from girdles to zeugopods (Fig. 4A-C, *centre*).
412 Figure 6 (A-C) shows the scatter plots of the first PLS axes obtained with the
413 size-free species averages and the morphological changes associated with them. In the
414 case of the scapula-pelvis comparison (Fig. 6A), the morphological change in the
415 scapula is the degree of robustness. Regarding the pelvis, as the scapula becomes more
416 robust, the iliac crest widens, the pubic symphysis and ischium both shorten, and the
417 ischial tuberosity undergoes increased dorsolateral projection (Fig. 6A). In this axis,
418 felids have slender scapulae and pelvises with narrow iliac crests. At the opposite
419 extreme, ursids have robust scapulae and pelvises with wide iliac crests.
420 The analyses of the stylopod (humerus-femur) and the zeugopod (radius-tibia)
421 were very similar (Figs. 6B-C). In both cases, the morphological change related to these
422 axes was the degree of bone robustness. Thus, a more robust stylopod/zeugopod in the
423 forelimb is associated with a more robust stylopod/zeugopod in the hind limb, and vice
424 versa. The distribution of species along these axes is very similar to the distributions
425 obtained for the within-limbs comparisons: most canids occupy the morphospace region

426 characterized by slender morphologies, whereas several ursids (especially *A.*
427 *melanoleuca* and *M. ursinus*) and mustelids (*M. meles* and *L. canadensis*) occupy the
428 region characterized by robust shapes.
429 (iii) Covariation between functionally equivalent bones
430 All the RV coefficients obtained from the comparisons of functionally
431 equivalent limb bones (i.e., ulna-tibia, scapula-femur, and humerus-tibia) were
432 statistically significant ($P < 0.01$). The RV coefficients and the percentages of
433 covariance explained by the first PLS axes (Table 3) obtained with the Procrustes
434 coordinates (Fig. 4A, *right*) and the size-free species averages (Fig. 4B, *right*) were
435 higher than those obtained with the size-free independent contrasts (Fig. 4C, *right*). In
436 this case, the highest RV value was obtained from the ulna-tibia comparison (Fig. 4A-C,
437 *right*) and the lowest one was obtained from the girdle comparison (i.e., scapula-femur).
438 The percentages of covariance explained by the first PLS axis for these comparisons
439 were similar (Table 3).
440 Figure 6D-F shows the scatter plots of the first PLS axes obtained with the size-
441 free species averages and the morphological changes associated with them. Again, these
442 morphological changes are related to the degree of bone robustness. Thus, the species
443 distribution was very similar in all the comparisons: canids usually have slender bones,
444 whereas the Northern river otter, ursids, and some felids have more robust ones (Fig.
445 6D-F).
446 (iv) Testing for similarity in the morphological covariation of all bone comparisons
447 As indicated by the angular comparison test (Table S3), all comparisons showed
448 that the first PLS axes for each of the pairs of bones were not statistically different using
449 the Procrustes coordinates or the size-free species averages data ($P < 0.05$). For
450 example, the shape covariance of the scapula associated with the femur is very similar

to the shape covariance of the scapula associated with the pelvis, and this applies to all pairs of bones. Therefore, the main aspects of shape covariance were basically similar in all between- and within-limbs comparisons.

Influence of functional specialization on the patterns of limb bone shape integration

Table 2 shows the results of the regressions of shape on size for each functional subsample (cursorial and non-cursorial taxa), and the results obtained for the presence of phylogenetic signal in the size-free shape variation. The graphic models shown in Figure 7 depict the RV coefficients obtained for all comparisons. The bootstrap test confirmed that there were significant differences in the RV coefficients between cursors and non-cursors in some of the comparisons. Figure 8 depicts the results of this bootstrap test and shows the random distribution of the RV differences obtained from the size-free species averages as well as the 90 and 95% bootstrap percentile intervals for the anatomically connected bones (Fig. 8A-F), between serial homologues (Fig. 8 G-I) and functional equivalents (Fig. 8J-L). Table 4 also shows the bootstrap percentile and the confidence intervals at the 90% and 95% levels for the size-free independent contrasts.

None of the within-limb comparisons using the size-free species averages were statistically different from zero, as the null difference was within the 90 and 95% percentile intervals in all cases (Figs. 8A-F). However, when the size-free independent contrasts data were used, the differences in RV values for the humerus-ulna, radius-ulna, pelvis-femur and femur-tibia comparisons were significantly different from zero at the 90% confidence interval (Table 4). Although this is not the usual level of statistical significance, it may suggest the presence of a general trend.

Regarding the between-limb comparisons, the differences in the RV coefficient between the comparisons of the serially homologous scapula-pelvis, humerus-femur and

radius-tibia (Figs. 8, 8H and 8I) were not significant for the size-free species averages. However, in the case of the radius-tibia comparison, the null values for the differences in the RV coefficients were outside the 95% confidence intervals for size-free independent contrasts (Table 4). The differences in the RV coefficients between cursors and non-cursors were not significant in the comparisons between functionally equivalent proximal bones (scapula-femur; Fig. 8K; Table 4). In contrast, the functional ulna-tibia comparison yielded significant results at the 90% percentile interval when the species averages data were used (Fig. 8J), and at the 95% confidence interval when the independent contrasts data were employed (Table 4). Similarly, the humerus-tibia comparison was significant at the 95% percentile interval (Fig 8L) for the size-free species averages and at the 95% confidence interval for the size-free independent contrasts (Table 4).

DISCUSSION

Patterns of limb covariation reveal a highly integrated appendicular skeleton in carnivorans

The results obtained from the PLS analyses and the RV coefficients show that the carnivoran appendicular skeleton is highly integrated to function as a whole. Furthermore, the angular comparison test indicated that shape covariance is related to the degree of bone robustness in all the comparisons, with the sole exception of the pelvis, which has a more complex shape variation. Thus, the axis of maximum shape covariance is strikingly similar to the main axes of shape variability that were obtained in previous studies of both limbs using principal components analyses for each appendicular bone (Martín-Serra et al. 2014a, 2014b). As expected, the distribution of species along the PLS axes generally resembles the distributions found in our previous studies (Martín-Serra et al. 2014a, 2014b). The high correspondence between the

maximum shape covariance (between bones) and the maximum shape variance (for each bone) confirms the remarkably tight integration of the carnivoran appendicular skeleton. In addition, although both allometry and phylogeny are significant sources of bone shape variation, they do not seem to strongly influence the patterns of morphological integration. In fact, although the strength of the association between elements was slightly reduced when the effects of phylogeny were taken into account, integration remained significant.

We hypothesize that this remarkable integration pattern could be partly due to the strong biomechanical constraints that terrestrial locomotion place on the major limb bones. This biomechanical constraint could be related to a trade-off between resistance to weight-bearing stresses (achieved by robust bones) and the maintenance of energetic efficiency during locomotion (achieved by slender bones), given that adaptations for economical locomotion are counterbalanced by those for increased strength (Pasi and Carrier 2003; Kemp et al. 2005; Martín-Serra et al. 2014a, 2014b). However, it is noteworthy that the data do not allow this trade-off to be rigorously tested, as the data are neither kinetic nor kinematic. Thus, given that all the species included in this study are quadrupedal, the bones of the fore- and hind limbs vary in a coordinated manner as a function of their robustness, because both limbs are affected by similar biomechanical needs. The most noteworthy exceptions are the northern river otter (a semi-aquatic species) and the European badger (a digging species), which is probably due to the fact that the functions of the fore- and hind limbs differ more in these species than in other carnivorans (Tarasoff 1972; Fish 1994).

Differences in the within- and between-limbs patterns of covariation

Despite the high degree of morphological integration between bones, the strength of this covariation is not constant throughout the appendicular skeleton. As

indicated by the RV coefficients of the comparisons between the serially homologous elements, the two girdles seem to be the least integrated elements, which could be related to their different evolutionary history compared to the long bones (Young 2004; Kardong 2006). However, although the shape covariance of the scapula with all other limb bones remains more or less constant and is associated with changes in robustness (Figs. 5A and 6A, E), the shape covariance of the pelvis with other bones is more variable (e.g., see Fig. 5E for the shape covariances of the pelvis and femur and Fig. 6A for those of the pelvis and scapula). This difference in the pattern of integration between both girdles is also supported by the low percentages of shape covariation explained by the first PLS axes in all comparisons (Table 3). A possible explanation for this result could be related to their structural differences relative to the axial skeleton: whereas the scapula is a mobile element, the pelvis is fixed to the vertebral column. Thus, the scapula contributes to stride length during locomotion (as do other long bones) and the pelvis anchors important hind limb muscles and transmits their movements to the trunk (Raich and Casinos 1991; Gasc 2001; Polly 2007; Williams et al. 2008; Schmidt and Fischer 2009; Hudson et al. 2011). According to this morpho-functional interpretation, the pelvis should not be expected to be as constrained as the scapula by the same type of biomechanical demands that primarily affect other limb bones. Alternatively, the pattern of covariance could be influenced by the fact that the pelvis is the result of the fusion of three different elements (ilium, ischium, and pubis). Although it is beyond the aims of this article to investigate the nature of the differences between both girdles, this topic deserves further in-depth study.

Another clear difference in the degree of shape covariation between serially homologous bones is that zeugopods (radius-tibia) appear to be more integrated than stylopods (humerus-femur). Developmental and functional reasons could underlie this

difference: due to the fact that as a limb bone is more distally positioned in the appendicular skeleton, its shape and dimensions are more subject to functional adaptations (Figueirido et al. 2011) and are less limited by developmental constraints because distal growth plates close later (Weisbecker et al. 2008; Weisbecker 2011; Geiger et al. 2014).

Similar results were obtained by the comparisons between functionally equivalent bones and between serially homologous bones. The strong covariation between the ulna and the tibia (Fig. 4) suggests that they may have undergone a certain degree of convergence in their functions. The results appear to partially support the alternative hypothesis concerning the displacement of functional equivalence in relation to serial homology (Raich and Casinos 1991, Gasc 2001, Schmidt and Fischer 2009). In fact, the humerus and tibia show high covariation (see Fig. 6, *right column*), which suggests that their functional equivalence may have a real effect on the morphological changes of these bones. In contrast, covariation between the scapula and the femur is weak (see Fig. 4, *right column*), which is probably due to their different developmental processes and timing (Geiger et al. 2014). Thus, the presumed functional equivalence between both bones does not have a substantial effect on their morphological covariation.

Functional specialization increases integration within and between limbs

As indicated by the bootstrap tests, the results suggest that the degree of integration in the appendicular skeleton seems to be higher in cursorial species than in non-cursorial ones. Furthermore, when phylogeny is taken into account, the appendicular skeleton of cursorial taxa remains more integrated than that of non-cursorial taxa, although to a lesser degree than when phylogeny is not taken into account (see Table 4). Although a more in-depth research is needed to find the processes that underlie this pattern (perhaps

576 comparing different levels of integration), following our results we hypothesize that it
577 may be due to the fact that cursors have a forelimb specialized for locomotion, whereas
578 non-cursors also use the forelimb for grappling prey, swimming, digging, or
579 manipulating food. Thus, whereas both limbs of cursors converge in their functions, the
580 limb functions of non-cursors diverge, which appears to be related to the lower degree
581 of integration between the appendicular elements. Furthermore, in cursorial taxa the
582 comparisons between distal functional equivalents (ulna-tibia and humerus-tibia; Fig. 8)
583 are more integrated and are more susceptible than other elements to modification by
584 functional causes. This finding is also supported when phylogeny is taken into account,
585 because these comparisons plus the radius-tibia appear as still more integrated in
586 cursors than in non-cursors (Table 4). The results indicate that the appendicular bones
587 are more integrated in species that specialize in locomotion and that such specialization
588 particularly affects the distal elements.
589 Young and Hallgrímsson (2005) and Bell et al. (2011) demonstrated a similar
590 process but in the opposite direction regarding the tight association between functional
591 specialization and morphological integration. They showed that the highly integrated
592 pattern between serially homologous elements decreases in specialized taxa with
593 extremely different limb functions (e.g., flying vertebrates). Thus, in this case,
594 functional specialization entails a divergence of functions between both limbs. The
595 particular developmental strategies of marsupial mammals also reduce limb integration
596 (Kelly and Sears 2010; Bennett and Goswami 2011). Marsupials are altricial and need
597 well-developed forelimbs to climb towards the mother's teat (Sears 2004). This
598 underlies the difference in developmental timing between the fore- and hind limb in
599 marsupials (Weisbecker et al 2008; Goswami et al. 2009; Sears 2009; Geiger et al.

2014) and, as a result, a reduced level of morphological integration (Kelly and Sears 2010; Bennett and Goswami 2011).

Strikingly, the case regarding the appendicular skeleton of carnivorans seems to be the opposite, as the ancestral condition of basal carnivorans is a less integrated appendicular skeleton and generalized morpho-functional limbs (Heinrich and Rose 1995, 1997, Heinrich and Houde 2006, Spaulding and Flynn 2009, Tomiya 2011, Samuels et al. 2013). Therefore, taxa specializing in cursorial locomotion lose the "non-locomotory" skills of their forelimb and increase the degree of integration between their limbs. More interestingly, the results also show that the pattern of integration may not only change due to large differences in function or development among distantly related clades (e.g., bats, birds and marsupials), but could also change due to subtle differences in function or development within closely related species at an evolutionary level.

CONCLUSIONS

This study investigated whether the pattern of evolutionary integration in the appendicular skeleton of mammalian carnivores was shaped by performance selection in terms of organismal function and, if so, how this pattern was influenced by allometry and phylogeny. The results indicate that the appendicular skeleton of carnivorans is highly integrated despite the effects of phylogeny and allometric effects. Anatomically connected bones (within limbs) and serial homologues or functionally equivalent elements (between limbs) are significantly integrated. Furthermore, the most important morphological change associated with bone covariance is the degree of bone robustness. The pelvis is an exception, which is probably due to its different evolutionary history, structure, and function relative to the scapula.

Strikingly, the degree of integration increases from the proximal girdles to the more distal bones both within and between the limbs. In addition, as functional

adaptations are more evident in the more distal bones, we hypothesized that functional factors could have played a role in shaping this pattern. The effects of functional adaptation were also indicated by comparing the strength of the covariation between pairs of anatomically connected bones, serial homologues, or functional equivalents in two different ecological groups: carnivoran species specialized for cursorial locomotion and non-cursorial taxa. The degree of integration between the distal elements is higher in cursors than in non-cursors. Thus, the loss of functions in the forelimb of cursorial taxa is associated with a higher degree of integration in the more distal elements of both limbs.

Our findings suggest that functional interactions between carnivoran appendicular elements can modify the patterns of morphological integration at an evolutionary level (see Fig. 1B). In other words, the developmental processes that underlie the formation of the appendicular skeleton have been modified to match functional associations through natural selection (Wagner and Altenberg 1996; Klingenberg 2014).

ACKNOWLEDGMENTS

We are especially grateful to C. M. Janis, and F. J. Serrano for their helpful suggestions during the writing of this paper. We thank M. Laurin for giving us statistical advice. We also thank J. X. Samuels and an anonymous reviewer for their insightful comments, which helped to improve the quality of the paper. Associate Editor P. D. Polly also contributed constructive remarks. We thank R. Portela (NHM, London) and E. Westwig (AMNH, New York) for kindly providing us with access to the specimens under their care, and to S. Almécija for providing us with the bone scanning surfaces. This study was supported by a PhD Research Fellowship (FPU) to AM-S from the “Ministerio de

Educación y Ciencia" and CGL2012-37866 grant to BF from the "Ministerio de Economía y Competitividad". The authors declare that there are no conflicts of interest.

LITERATURE CITED

Andersson, K. 2003. Locomotor evolution in the Carnivora (Mammalia): evidence from the elbow joint. Doctoral dissertation, Department of Earth Sciences, Hist. Geol. and Pal, University of Uppsala, Sweden.

Andersson, K. 2004. Predicting carnivoran body mass from a weight-bearing joint. J. Zool. 262:161–172.

Andersson, K. 2005. Were there pack-hunting canids in the Tertiary, and how can we know? Paleobiology 31:56–72.

Andersson K, and L. Werdelin. 2003. The evolution of cursorial carnivores in the Tertiary: implications of elbow-joint morphology. Proc. R. Soc. Lond. B. (Suppl.) 270:S163–S165.

Anyonge, W. 1996. Locomotor behaviour in Plio-Pleistocene sabre-tooth cats: a biomechanical analysis. J. Zool. 238:395–413.

Arthur, W. 2001. Developmental drive: an important determinant of the direction of phenotypic evolution. Evol. Dev. 3:271–278.

Audet, A. M., C. B. Robbins, and S. Lariviere. 2002. *Alopex lagopus*. Mamm. Spec. 713:1–10.

Bekoff, M. 1977. *Canis latrans*. Mamm. Spec. 79:1–9.

Bell, E., B. Andres, and A. Goswami. 2011. Integration and dissociation of limb elements in flying vertebrates: a comparison of pterosaurs, birds and bats. J. Evol. Biol. 24:2586–2599.

Bennett, C. V., and A. Goswami. 2011. Does developmental strategy drive limb integration in marsupials and monotremes? Mammal. Biol. 76:79–83.

674 Berta, A. 1982. *Cerdocyon thous*. Mamm. Spec. 186:1–4.
675 Bestelmeyer, S. V., and C. Westbrook. 1998. Maned wolf (*Chrysocyon brachyurus*)
676 predation on pampas deer (*Ozotoceros bezoarticus*) in Central Brazil. Mammalia
677 62:591–595.
678 Bieseigel, B. D., G. L. Zuercher. 2005. *Speothos venaticus*. Mamm. Spec. 783:1–6.
679 Bininda-Emonds, O. R., J. E. Jeffery, M. R. Sánchez-Villagra, J. Hanken, M. Colbert,
680 C. Pieau, L. Selwood, C. ten Cate, A. Raynaud, C. K. Osabutey, and M. K. Richardson.
681 2007. Forelimb-hindlimb developmental timing changes across tetrapod phylogeny.
682 BMC Evol Biol. 7:182.
683 Breuker, C. J., V. Debat, and C. P. Klingenberg. 2006. Functional evo-devo. Trends
684 Ecol. Evol. 21:488–492.
685 Chamero, B., Á. D. Buscalioni, and J. Marugán-Lobón. 2013. Pectoral girdle and
686 forelimb variation in extant Crocodylia: the coracoid–humerus pair as an evolutionary
687 module. Biol. J. Linn. Soc. Lon. 108:600–618.
688 Chan, W. 2009. Bootstrap Standard Error and Confidence Intervals for the Difference
689 Between Two Squared Multiple Correlation Coefficients. Educ. Psychol. Meas.
690 69:566–584.
691 Chapman, J. A., and G. A. Feldhamer. 1982. Wild mammals of North America. Johns
692 Hopkins Press, Baltimore, U.S.
693 Cheverud, J. M. 1982. Relationships among ontogenetic, static, and evolutionary
694 allometry. Am. J. Phys. Anthropol. 59:139–149.
695 Cheverud, J. M. 1996. Developmental integration and the evolution of pleiotropy. Am.
696 Zool. 36:44–50.
697 Chorn, J, and R. S. Hoffmann. 1978. *Ailuropoda melanoleuca*. Mamm. Spec. 110:1–6.
698 Clark, H. O. Jr. 2005. *Otocyon megalotis*. Mamm. Spec. 766:1–5.

699 Cohen, J. A. 1978. *Cuon alpinus*. Mamm. Spec. 100:1–3.

700 Currier, M. J. P. 1983. *Felis concolor*. Mamm. Spec. 200:1–7.

701 Demaster, D. P., and I. Stirling. 1981. *Ursus maritimus*. Mamm. Spec. 45:1–7.

702 Díaz-Uriarte, R., and T. Garland. 1998. Effects of branch length errors on the

703 performance of phylogenetically independent contrasts. Syst. Biol. 47: 654–672.

704 Dietz, J. M. 1985. *Chrysocyon brachyurus*. Mamm. Spec. 234:1–4.

705 Drake, A.G., and C. P. Klingenberg. 2008. The pace of morphological change:

706 historical transformation of skull shape in St Bernard dogs. Proc. R. Soc. Lond. B. Biol.

707 Sci. 275:71–76.

708 Dryden, I. L., and K. Mardia. 1998. Statistical Analysis of Shape. Wiley, Chichester,

709 U.K.

710 Escoufier, Y. 1973. Le traitement des variables vectorielles. Biometrics 29:751–760.

711 Ewer, R.F. 1973. The Carnivores. Cornell University Press, Ithaca, N.Y.

712 Fabre, A-C., R. Cornette, G. Slater, C. Argot, S. Peigné, A. Goswami, and E.

713 Pouydebat. 2013. Getting a grip on the evolution of grasping in musteloid carnivorans:

714 a three-dimensional analysis of forelimb shape. J. Evol. Biol. 26:1521–1535.

715 Fabre, A-C., A. Goswami, S. Peigné, and R. Cornette. 2014. Morphological integration

716 in the forelimb of musteloid carnivorans. J. Anat. 225:19–30

717 Felsenstein, J. J. 1985. Phylogenies and the comparative method. Am. Nat. 125:1–15.

718 Figueirido, B., and C. M. Janis. 2011. The predatory behaviour of the thylacine:

719 Tasmanian tiger or marsupial wolf? Biol. Lett. 7: 937–940.

720 Figueirido, B., J. A. Pérez-Claros, R. M. Hunt Jr, and P. Palmqvist. 2011. Body mass

721 estimation in amphicyonid carnivoran mammals: A multiple regression approach from

722 the skull and skeleton. Acta Palaeontol. Pol. 56:225–246.

723 Figueirido, B., Z. J. Tseng, and A. Martín-Serra. 2013. Skull shape evolution in
724 durophagous carnivorans. Evolution 67:1975–1993.
725 Fish, F. E. 1994. Association of propulsive swimming mode with behavior in river
726 otters (*Lutra canadensis*). J. Mammal. 55:989–997.
727 Fitzgerald, C. S, and P.R. Krausman. 2002. *Helarctos malayanus*. Mamm. Spec. 696:1–
728 5.
729 Ford, L. S., and R. S. Hoffman. 1988. *Potos flavus*. Mamm. Spec. 321:1–9.
730 Futuyma, D. J. 2010. Evolutionary constraint and ecological consequences. Evolution
731 64:1865–1884.
732 Gasc, J.-P. 2001. Comparative aspects of gait, scaling and mechanics in mammals.
733 Comp. Biochem. Physiol. A 131:121–133.
734 Geiger, M., A. M. Forasiepi, D. Koyabu, and M. R. Sánchez-Villagra. 2014.
735 Heterochrony and post-natal growth in mammals–an examination of growth plates in
736 limbs. J. Evol Biol. 27:98–115.
737 Gidaszewski, N.A., M. Baylac, C. P. Klingenberg. 2009. Evolution of sexual
738 dimorphism of wing shape in the *Drosophila melanogaster* subgroup. BMC Evol. Biol.
739 9:110.
740 Gompper, M. E., and D. M. Decker. 1998. *Nasua nasua*. Mamm. Spec 580:1–9.
741 Gonyea, W. J. 1978. Functional implications of felid forelimb morphology. Acta Anat.
742 102:111–121.
743 Goswami, A. 2006a. Morphological integration in the carnivoran skull. Evolution
744 60:169–183.
745 Goswami, A. 2006b. Cranial modularity shifts during mammalian evolution. Am. Nat.
746 168:270–280.

747 Goswami, A., and P. D. Polly. 2010a. The influence of modularity on cranial
748 morphological disparity in Carnivora and Primates (Mammalia). PLoS ONE 5:e9517.
749 Goswami, A., and P.D. Polly. 2010b. Methods for studying morphological integration
750 and modularity. Pp. 213–243 *in* J. Alroy and G. Hunt, eds. Quantitative Paleontology.
751 Paleontological Society Short Course, October 30th, 2010. The Paleontological Society
752 Papers, Volume 16.
753 Goswami, A., J. B. Smaers, C. Soligo, and P. D. Polly. 2014. The macroevolutionary
754 consequences of phenotypic integration: from development to deep time. Phil. Trans. R.
755 Soc. B 369:20130254.
756 Goswami, A., V. Weisbecker, and M. R. Sánchez-Villagra. 2009. Developmental
757 modularity and the marsupial-placental dichotomy. J. Exp. Zool. 312B:186–195.
758 Haas, S. K., V. Hayssen, and P. R. Krausman. 2005. *Panthera leo*. Mamm. Spec.
759 762:1–11
760 Hallgrímsson, B., H. Jamniczky, N. M. Young, C. Rolian, T. E. Parsons, J. C.
761 Boughner, and R. S. Marcucio. 2009. Deciphering the palimpsest: studying the
762 relationship between morphological integration and phenotypic covariation. Evol.
763 Biol. 36:355–376.
764 Hallgrímsson, B., K. Willmore, and B. K. Hall. 2002. Canalization, developmental
765 stability, and morphological integration in primate limbs. Yearb. Phys. Anthropol.
766 45:131–158.
767 Hansen, T. F. 2003. Is modularity necessary for evolvability? Remarks on the
768 relationship between pleiotropy and evolvability. BioSistems 69:83–94
769 Heinrich, R. E., and P. Houde. 2006. Postcranial anatomy of *Viverravus* (Mammalia,
770 Carnivora) and implications for substrate use in basal Carnivora. J. Vertebrate
771 Paleontol. 26:422–435.

772 Heinrich, R. E., and K. D. Rose. 1995. Partial skeleton of the primitive carnivoran
773 *Miacis petilus* from the early Eocene of Wyoming. J. Mammal. 76:148–162.
774 Heinrich, R. E., and K. D. Rose. 1997. Postcranial morphology and locomotor
775 behaviour of two Early Eocene miacoid carnivorans, *Vulpavus* and *Didymictis*.
776 Palaeontology 40:279–305.
777 Hemmer, H. 1972. *Uncia uncia*. Mamm. Spec. 20:1–5.
778 Hildebrand, M. 1985. Walking and running. Pp. 38–57 *in* M. Hildebrand, D.M.
779 Bramble, K.F. Liem and D.B. Wake, eds. Functional vertebrate morphology. Belknap,
780 Harvard. Cambridge, MS, US.
781 Hudson, P. E., S. A. Corr, R. C. Payne-Davis, S. N. Clancy, E. Lane, and A. M. Wilson.
782 2011. Functional anatomy of the cheetah (*Acinonyx jubatus*) hindlimb. J. Anat.
783 218:363–374.
784 Iwaniuk, A. N., and I. Q. Whishaw. 1999. How skilled are the skilled limb movements
785 of the raccoon (*Procyon lotor*)? Behav. Brain Res. 99:35–44.
786 Iwaniuk, A. N., and I. Q. Whishaw. 2000. On the origin of skilled forelimb movements.
787 Trends Neurosci. 23:372–376.
788 Iwaniuk, A.N., S. M. Pellis, and I. Q. Whishaw. 1999. The relationship between
789 forelimb morphology and behaviour in North American carnivores (Carnivora). Can. J.
790 Zool. 77:1064–1074.
791 Iwaniuk, A.N., S. M. Pellis, and I. Q. Whishaw. 2000. The relative importance of body
792 size, phylogeny, locomotion, and diet in the evolution of forelimb dexterity in fissiped
793 carnivores (Carnivora). Can. J. Zool. 78:1110–1125.
794 Janis, C. M., and B. Figueirido. 2014. Forelimb anatomy and the discrimination of the
795 predatory behavior of carnivorous mammals: The thylacine as a case study. J. Morphol.
796 doi: 10.1002/jmor.20303

797 Janis, C. M., and P. B. Wilhelm. 1993. Were there mammalian pursuit predators in the
798 Tertiary? Dances with wolf avatars. J. Mammal. Evol. 1:103–125.
799 Jenkins, F. A. 1974. The movement of the shoulder in claviculate and aclaviculate
800 mammals. J. Morphol. 144:71–83.
801 Kardong, K. V. 2006. Vertebrates: comparative anatomy, function, evolution. McGraw-
802 Hill, Boston, US.
803 Kelly, E. M., and K. E. Sears. 2011. Reduced phenotypic covariation in marsupial limbs
804 and the implications for mammalian evolution. Biol. J. Linn. Soc. Lon. 102:22–36.
805 Kemp, T. J., K. N. Bachus, J. A. Nairn, and D. R. Carrier. 2005. Functional trade-offs in
806 the limb bones of dogs selected for running versus fighting. J. Exp. Biol. 208:3475–
807 3482.
808 Kingdon, J. 1988. East African Mammals: An Atlas of Evolution in Africa, Vol. 3, Part
809 A: Carnivores. University of Chicago Press, Chicago, US.
810 Kleiman, D. G. 1972. Social behavior of the maned wolf (*Chrysocyon brachyurus*) and
811 bush dog (*Speothos venaticus*): a study in contrast. J. Mammal. 53:791–806.
812 Klingenberg, C. P. 2008. Morphological integration and developmental modularity.
813 Annu. Rev. Ecol. Evol. Syst. 39:115–132.
814 Klingenberg, C. P. 2009. Morphometric integration and modularity in configurations of
815 landmarks: tools for evaluating a priori hypotheses. Evol. Dev. 11:405–421.
816 Klingenberg, C. P. 2010. Evolution and development of shape: integrating quantitative
817 approaches. Nat. Rev. Genet. 11:623–635.
818 Klingenberg, C. P. 2011. MorphoJ. Faculty of Life Sciences, University of Manchester,
819 Manchester. Available from: http://www.flywings.org.uk/MorphoJ_page.htm.
820 Klingenberg, C. P. 2013. Cranial integration and modularity: insights into evolution and
821 development from morphometric data. Hystrix 24:43–58.

822 Klingenberg, C. P. 2014. Studying morphological integration and modularity at multiple
823 levels: concepts and analysis. Phil. Trans. R. Soc. B 369:20130249.
824 Klingenberg, C. P., and N. A. Gidaszewski. 2010. Testing and quantifying phylogenetic
825 signals and homoplasy in morphometric data. Syst. Biol. 59:245-261.
826 Klingenberg, C. P., and J. Marugán-Lobón. 2013. Evolutionary Covariation in
827 Geometric Morphometric Data: Analyzing Integration, Modularity, and Allometry in a
828 Phylogenetic Context. Syst. Biol. 62:591-610.
829 Klingenberg, C. P., and G. S. McIntyre. 1998. Geometric morphometrics of
830 developmental instability: analyzing patterns of fluctuating asymmetry with Procrustes
831 methods. Evolution 52:1363-1375.
832 Klingenberg, C. P., and S. D. Zaklan. 2000. Morphological integration between
833 developmental compartments in the *Drosophila* wing. Evolution 54:1273–1285.
834 Klingenberg, C. P., and M. Zimmermann. 1992. Static, ontogenetic, and evolutionary
835 allometry: a multivariate comparison in nine species of water striders. Am. Nat.
836 140:601–620.
837 Koepfli, K. P., M. E. Gompper, E. Eizirik, C. C. Ho, L. Linden, J. E. Maldonado, and R.
838 K. Wayne. 2007. Phylogeny of the Procyonidae (Mammalia: Carnivora): molecules,
839 morphology and the great American interchange. Mol. Phylogenet. Evol. 43:1076–
840 1095.
841 Krausman, P. R., and S. M. Morales. 2005. *Acinonyx jubatus*. Mamm. Spec. 771:1–6.
842 Langguth, A. 1975. Ecology and evolution in the South American canids. Pp. 192-206
843 *in* M. V. Fox, ed. The wild canids: their systematics, behavioural ecology and evolution.
844 Van Nostrand Reinhold Co. New York, USA.
845 Lariviére, S. 2001. *Ursus americanus*. Mamm. Spec. 647:1–11.
846 Lariviére, S., and L. R. Walton. 1997. *Lynx rufus*. Mamm. Spec. 563:1–8.

847 Lariviére, S., and L. R. Walton. 1998. *Lontra canadensis*. Mamm. Spec. 587:1–8.
848 Laurin, M. 2004. The evolution of body size, Cope's rule and the origin of amniotes.
849 Syst. Biol. 53:594–622.
850 Lawler, R. R. 2008. Morphological integration and natural selection in the postcranium
851 of wild Verreaux's sifaka (*Propithecus verreauxi verreauxi*). Am. J. Phys.
852 Anthropol. 136:204–213.
853 Lotze, J. H., and S. Anderson. 1979. *Procyon lotor*. Mamm. Spec. 119:1–8.
854 Macdonald, D. W., and J. C. Reynolds. 2004. Red fox (*Vulpes vulpes*). Pp. 129–136 *in*
855 C. Sillero-Zubiri, M. Hoffmann, and D. W. Macdonald, eds. Canids: foxes, wolves,
856 jackals, and dogs: status survey and conservation action plan. IUCN, Gland,
857 Switzerland and Cambridge, UK.
858 Maddison, W.P., and D. R. Maddison. 2011. Mesquite: a modular system for
859 evolutionary analysis. Version 2.75. Available via http://mesquiteproject.org.
860 Magwene, P. M. 2001. New tools for studying integration and modularity. Evolution
861 55:1734–1745.
862 Manly, B. F. J. 2007. Randomization, Bootstrap and Monte Carlo Methods in Biology.
863 Chapman and Hall–CRC, Boca Raton, US.
864 Martín-Serra, A., B. Figueirido, and P. Palmqvist. 2014a. A three-dimensional analysis
865 of morphological evolution and locomotor performance of the carnivoran
866 forelimb. PloS one 9:e85574.
867 Martín-Serra, A., B. Figueirido, and P. Palmqvist. 2014b. A three-dimensional analysis
868 of the morphological evolution and locomotor behaviour of the carnivoran hind limb.
869 BMC Evol. Biol. 14:129.
870 Mazák, V. 1981. *Panthera tigris*. Mamm. Spec. 152:1–8.

McMahon, T. A. 1975. Allometry and biomechanics: limb bones in adult ungulates. Am. Nat. 109:547–563.

Mech, L. D. 1974. *Canis lupus*. Mamm. Spec. 37:1–6.

Meloro, C., S. Elton, J. Louys, L. C. Bishop, and P. Ditchfield. 2013. Cats in the forest: predicting habitat adaptations from humerus morphometry in extant and fossil Felidae (Carnivora). Paleobiology 39:323–344.

Mezey, J. G., J. M. Cheverud, and G. P. Wagner. 2000. Is the genotype-phenotype map modular?: a statistical approach using mouse quantitative trait loci data. Genetics 156:305–311.

Mills, M. G. L. 1982. *Hyaena brunnea*. Mamm. Spec. 194:1–6.

Moehrenschlager, A., and M. Sovada. 2004. Swift fox (*Vulpes velox*). Pp. 109–116 *in* C. Sillero-Zubiri, M. Hoffmann, and D. W. Macdonald, eds. Canids: foxes, wolves, jackals, and dogs: status survey and conservation action plan. IUCN, Gland, Switzerland and Cambridge, UK.

Monteiro, L. R. 1999. Multivariate regression models and geometric morphometrics: the search for causal factors in the analysis of shape. Syst. Biol. 48:192–199

Monteiro, L. R., V. Bonato, and S. F. Dos Reis. 2005. Evolutionary integration and morphological diversification in complex morphological structures: mandible shape divergence in spiny rats (Rodentia, Echimyidae). Evol. Dev. 7:429–439.

Nowak, R. M. 1999. Walker's Carnivores of the World 7th ed. John Hopkins University Press. Baltimore, MD, US.

Nyakatura, K., and O. R. P. Bininda-Emonds. 2012. Updating the evolutionary history of Carnivora (Mammalia): a new species-level supertree complete with divergence time estimates. BMC Biol. 10:12.

895 Olson, E. C., and R. A. Miller. 1951. A mathematical model applied to a study of the
896 evolution of species. Evolution 5:256–338.
897 Olson, E. C., and R. A. Miller. 1958. Morphological integration. University of Chicago
898 Press, Chicago, US.
899 Pasi, B. M., and D. R. Carrier. 2003. Functional trade-offs in the limb muscles of dogs
900 selected for running versus fighting. J. Evol. Biol. 16:324–332.
901 Pasitschniak-Arts, M. 1993. *Ursus arctos*. Mamm. Spec. 439:1–10.
902 Piras, P., L. Maiorino, L. Teresi, C. Meloro, F. Lucci, T. Kotsakis, and P. Raia. 2013.
903 Bite of the Cats: Relationships between Functional Integration and Mechanical
904 Performance as Revealed by Mandible Geometry. Syst. Biol. 62:878–900.
905 Poglayen-Neuwall, I., and D. E. Toweill. 1988. *Bassariscus astutus*. Mamm. Spec.
906 327:1–8.
907 Polly, P. D. 2007. Limbs in mammalian evolution. Pp. 245-268 *in* B. K. Hall, ed. Fins
908 into Limbs: Evolution, Development and Transformation. University of Chicago Press,
909 Chicago, US.
910 Presley, S.J. 2000. *Eira barbara*. Mamm. Spec. 636:1–6.
911 Raich, J., and A. Casinos. 1991. Limb proportions in terrestrial mammals. Belg. J. Zool.
912 121:295-314.
913 Rieger, I. 1981. *Hyaena hyaena* Mamm. Spec. 150:1–5.
914 Roberts, M. S., and J. L. Gittleman. 1984. *Ailurus fulgens*. Mamm. Spec. 222:1–8.
915 Rodden, M., F. Rodrigues, and S. Bestelmeyer. 2004. Maned wolf (*Chrysocyon*
916 *brachyurus*). Pp. 38–43 *in* C. Sillero-Zubiri, M. Hoffmann, and D. W. Macdonald, eds.
917 Canids: foxes, wolves, jackals, and dogs: status survey and conservation action plan.
918 IUCN, Gland, Switzerland and Cambridge, UK.

919 Rohlf, F. J., and M. Corti. 2000. Use of two-block partial least-squares to study
920 covariation in shape. Syst. Biol. 49:740–753.
921 Rohlf, F. J., and L. F. Marcus. 1993. A revolution morphometrics. Trends Ecol. Evol.
922 8:129–132.
923 Samuels, J. X., J. A. Meachen, and S. A. Sakai. 2013. Postcranial morphology and the
924 locomotor habits of living and extinct carnivorans. J. Morphol. 274:121–146.
925 Schmidt, M., and M. S. Fischer. 2009. Morphological integration in mammalian limb
926 proportions: dissociation between function and development. Evolution 63:749–766.
927 Schoenebeck, J. J., S. A. Hutchinson, A. Byers, H. C. Beale, B. Carrington, D. L.
928 Faden, M. Rimbault, B. Decker, J. M. Kidd, R. Sood, et al. 2012. Variation of BMP3
929 Contributes to Dog Breed Skull Diversity. PLoS Genet 8:e1002849.
930 doi:10.1371/journal.pgen.1002849
931 Schutz, H, and R. P. Guralnick. 2007. Postcranial element shape and function: assessing
932 locomotor mode in extant and extinct mustelid carnivorans. Zool. J. Linnean Soc.
933 150:895–914.
934 Sears, K. E. 2004. Constraints on the morphological evolution of marsupial shoulder
935 girdles. Evolution 58:2353–2370.
936 Sears, K. E. 2009. Differences in the timing of early limb development in mammals: the
937 marsupial-placental dichotomy resolved. Evolution 63:2193–2200.
938 Seymour, K. L. 1989. *Panthera onca*. Mamm. Spec. 340:1–9.
939 Sillero-Zubiri, C., and J. Marino. 2004. Ethiopian wolf (*Canis simensis*). Pp. 167–174 *in*
940 C. Sillero-Zubiri, M. Hoffmann, and D. W. Macdonald, eds. Canids: foxes, wolves,
941 jackals, and dogs: status survey and conservation action plan. IUCN, Gland,
942 Switzerland and Cambridge, UK.

943 Singleton, M. 2012. Postnatal cranial development in papionin primates: An alternative
944 model for hominin evolutionary development. Evol. Biol. 39:499–520.
945 Spaulding, M., and J. J. Flynn. 2009. Anatomy of the postcranial skeleton of "*Miacis*"
946 *uintensis* (Mammalia: Carnivoramorpha). J. Vertebrate Paleontol. 29:1212–1223.
947 Sunquist, M., and F. Sunquist. 2002. Wildcats of the World. University of Chicago
948 Press, Chicago, US.
949 Taylor, M. E. 1989. Locomotor adaptations by carnivores. Pp. 382–409 *in* J. L.
950 Gittleman, ed. Carnivore behavior, ecology, and evolution. Cornell University Press,
951 Ithaca, NY. US.
952 Tarasoff, F. J. 1972. Comparative aspects of the hind limbs of the river otter, sea otter,
953 and seals. Pp. 333–359 *in* R. J. Harrison, ed. Functional Anatomy of Marine Mammals.
954 Academic Press. New York, U.S.
955 Tickle, C. 2002. Vertebrate limb development and possible clues to diversity in limb
956 form. J. Morphol. 252:252–237.
957 Tomiya, S. 2011. A new basal caniform (Mammalia: Carnivora) from the Middle
958 Eocene of North America and remarks on the phylogeny of early carnivorans. PLoS
959 ONE 6:e24146. doi:10.1371/journal.pone.0024146.
960 Trapp, G. R., D. L. Hallberg. 1975. Ecology of the gray fox (*Urocyon*
961 *cinereoargenteus*): a review. Pp. 164–178 *in* M. W. Fox, ed. The wild canids. Van
962 Nostrand Reinhold Co., New York, US.
963 Van Valen, L. 1965. The study of morphological integration. Evolution 19:347–349.
964 Van Valkenburgh, B. 1985. Locomotor diversity within past and present guilds of large
965 predatory mammals. Paleobiology 11:406–428.
966 Van Valkenburgh, B. 1987. Skeletal indicators of locomotor behavior in living and
967 extinct carnivores. J. Vertebrate Paleontol. 7:162–182.

968 Wagner, G. P. 1996. Homologues, natural kinds and the evolution of modularity. Am.
969 Zool. 36:36–43.
970 Wagner, G. P., and L. Altenberg. 1996. Complex adaptations and the evolution of
971 evolvability. Evolution 50:967–976.
972 Wagner, G. P., M. Pavlicev, and J. Cheverud. 2007. The road to modularity. Nat. Genet.
973 8:921–931.
974 Walmsley A, S. Elton, J. Louys, L. C. Bishop, and C. Meloro. 2012. Humeral
975 epiphyseal shape in the felidae: the influence of phylogeny, allometry, and locomotion.
976 J. Morphol. 273:1424–1438.
977 Walton, L. R., and D. O. Joly. 2003. *Canis mesomelas*. Mamm. Spec. 715:1–9.
978 Ward, O. G., and D. H. Wurster-Hill. 1990. *Nyctereutes procyonoides*. Mamm. Spec.
979 358:1–5.
980 Weisbecker, V. 2011. Monotreme ossification sequences and the riddle of mammalian
981 skeletal development. Evolution 65:1323–1335.
982 Weisbecker, V., A. Goswami, S. Wroe, and M. R. Sánchez-Villagra. 2008. Ossification
983 heterochrony in the therian postcranial skeleton and the marsupial-placental dichotomy.
984 Evolution 62:2027–2041.
985 Wiley, D. F., N. Amenta, D. A. Alcantara, D. Ghosh, Y. J. Kil, E. Delson, W. Harcourt-
986 Smith, F. J. Rohlf, K. St. John, B. Hamann. 2005. Evolutionary Morphing. Pp. 431–438
987 *in* Proceedings of IEEE Visualization 2005 (VIS'05).
988 Williams, S. B., J. R. Usherwood, K. Jespers, A. J. Channon, and A. M. Wilson. 2009.
989 Exploring the mechanical basis for acceleration: pelvic limb locomotor function during
990 accelerations in racing greyhounds (*Canis familiaris*). J. Exp. Biol. 212:550–565.
991 Wolfram, S. 2005. Mathematica 5.2, Wolfram Research, Inc., Champaign, IL, US.

992 Young, N. 2004. Modularity and integration in the hominoid scapula. J. Exp. Zool.
993 302:226-240.
994 Young, N. M., and B. Hallgrímsson. 2005. Serial homology and the evolution of
995 mammalian limb covariation structure. Evolution 59:2691–2704.
996 Young, R. L., and A. V. Badyaev. 2006. Evolutionary persistence of phenotypic
997 integration: influence of developmental and functional relationships on complex trait
998 evolution. Evolution 60:1291–1299.
999 Zelditch, M. L., D. L. Swiderski, H. D. Sheets, and W. L. Fink. 2004. Geometric
1000 morphometrics for biologists: a primer. Elsevier, San Diego, U.S.
1001 Zuercher, G.L., M. Swarner, L. Silveira, and O. Carrillo. 2004. Bush dog (*Speothos*
1002 *venaticus*). Pp. 76–80 *in* C. Sillero-Zubiri, M. Hoffmann, and D. W. Macdonald, eds.
1003 Canids: foxes, wolves, jackals, and dogs: status survey and conservation action plan.
1004 IUCN, Gland, Switzerland and Cambridge, UK.
1005
1006

TABLE AND FIGURE LEGENDS

Table 1. Species used in this study. The number of specimens per species is indicated. Bones that were absent in some specimens are shown in parenthesis. Abbreviations: S, scapula; P, pelvis; T, tibia. The functional classification of each species was established according to the following references: 1, Roberts and Gittleman (1984); 2, Nowak (1999); 3, Kingdon (1988); 4, Bekoff (1977); 5, Mech (1974); 6, Walton and Joly (2003); 7, Sillero-Zubiri and Marino (2004); 8, Berta (1982); 9, Dietz (1985); 10, Cohen (1978); 11, Ward and Wurster-Hill (1990); 12, Clark (2005); 13, Zuercher et al. (2004); 14, Chapman and Feldhamer (1982); 15, Audet et al. (2002); 16, Moehrenschlager and Sovada (2004); 17, Macdonald and Reynolds (2004); 18, Presley (2000); 19, Lariviére and Walton (1998); 20, Poglayen-Neuwall and Toweill (1988); 21, Gomper and Decker (1998); 22, Ford and Hoffman (1988); 23, Lotze and Anderson (1979); 24, Chorn and Hoffman (1978); 25, Fitzgerald and Krausman (2002); 26, Lariviére (2001); 27, Pasitschniak-Arts (1993); 28, Demaster and Stirling (1981); 29, Krausman and Morales (2005); 30, Lariviére and Walton (1997); 31, Sunquist and Sunquist (2002); 32, Haas et al. (2005); 33, Seymour (1989); 34, Mazák (1981); 35 Currier (1983); 36, Hemmer (1972); 37, Mills (1982); 38, Rieger (1981).

Family	Species (abbreviation)	N	Functional category
Ailuridae	*Ailurus fulgens (Afu)*	2	Non-cursor[1]
Canidae	*Canis adustus (Cad)*	1	Cursor[2]
	Canis aureus (Cau)	2	Cursor[3]
	Canis latrans (Cla)	5	Cursor[4]
	Canis lupus (Clu)	5	Cursor[5]
	Canis mesomelas (Cme)	4	Cursor[6]
	Canis simensis (Csi)	1	Cursor[7]
	Cerdocyon thous (Cth)	5	Cursor[8]
	Chrysocyon brachyurus (Cbr)	2	Cursor[9]
	Cuon alpinus (Cal)	4	Cursor[10]
	Lycaon pictus (Lpi)	2	Cursor[3]
	Nyctereutes procyonoides (Npr)	2	Non-cursor[11]
	Otocyon megalotis (Ome)	2	Cursor[12]
	Speothos venaticus (Sve)	2 (1 T)	Non-cursor[13]
	Urocyon cinereoargenteus (Uci)	4	Non-cursor[14]
	Vulpes lagopus (Vla)	2	Cursor[15]
	Vulpes velox (Vve)	2	Cursor[16]
	Vulpes vulpes (Vvu)	3	Cursor[17]
Mustelidae	*Eira barbara (Eba)*	2	Non-cursor[18]
	Lontra canadensis (Lca)	2	Non-cursor[19]
	Meles meles (Mme)	1	Non-cursor[2]
Procyonidae	*Bassariscus astutus (Bas)*	1	Non-cursor[20]
	Nasua nasua (Nna)	1	Non-cursor[21]
	Potos flavus (Pfl)	3	Non-cursor[22]
	Procyon lotor (Plo)	3	Non-cursor[23]
Ursidae	*Ailuropoda melanoleuca (Ame)*	4 (3 S)	Non-cursor[24]
	Helarctos malayanus (Hma)	1	Non-cursor[25]
	Melursus ursinus (Mur)	3	Non-cursor[2]
	Tremarctos ornatus (Tor)	1	Non-cursor[2]
	Ursus americanus (Uam)	3	Non-cursor[26]
	Ursus arctos (Uar)	4	Non-cursor[27]
	Ursus maritimus (Uma)	4 (2 P)	Non-cursor[28]
	Ursus thibetanus (Uth)	3	Non-cursor[2]
Felidae	*Acinonyx jubatus (Aju)*	5	Cursor[29]
	Leptailurus serval (Lse)	2 (1 P)	Non-cursor[2]
	Lynx rufus (Lru)	4	Non-cursor[30]
	Neofelis nebulosa (Nne)	1	Non-cursor[31]
	Panthera leo (Ple)	5	Non-cursor[32]
	Panthera onca (Pon)	4 (3 P)	Non-cursor[33]
	Panthera pardus (Ppa)	6 (5 P)	Non-cursor[2]
	Panthera tigris (Pti)	4	Non-cursor[34]
	Puma concolor (Pco)	4	Non-cursor[35]
	Uncia uncia (Uun)	4	Non-cursor[36]
Hyaenidae	*Crocuta crocuta (Ccr)*	5	Cursor[2]
	Hyaena brunnea (Hbr)	1	Cursor[37]
	Hyaena hyaena (Hhy)	2	Cursor[38]

Table 2. Results obtained for the regressions between shape and size and for the phylogenetic signal test of shape with the Principal Components. For regressions, the percentage of shape explained by size differences is indicated. The tree length is indicated for the phylogenetic signal tests. *P*-value between brackets. Asterisks indicate significant cases.

		Size-shape regression	Phylogenetic signal for shape
All	Scapula	14.29* (<0.01)	0.162* (<0.01)
	Humerus	13.22* (<0.01)	0.053* (<0.01)
	Radius	12.97* (<0.01)	0.039* (<0.01)
	Ulna	14.78* (<0.01)	0.064* (<0.01)
	Pelvis	11.5* (<0.01)	0.294* (<0.01)
	Femur	6.09* (0.02)	0.044* (<0.01)
	Tibia	6.19 (0.06)	0.027* (<0.01)
Cursors	Scapula	18.52%* (<0.01)	0.043* (<0.01)
	Humerus	17.66% (0.06)	0.014* (<0.01)
	Radius	14.7%* (0.04)	0.009 (0.1)
	Ulna	12.03% (0.09)	0.011* (0.03)
	Pelvis	13.24% (0.05)	0.104* (<0.01)
	Femur	13.88%* (0.04)	0.009* (0.01)
	Tibia	2.51% (0.6)	0.007* (<0.01)
Non-cursors	Scapula	21.97* (<0.01)	0.121* (<0.01)
	Humerus	19.41* (<0.01)	0.037* (<0.01)
	Radius	24.61* (<0.01)	0.026* (<0.01)
	Ulna	25.69* (<0.01)	0.045* (<0.01)
	Pelvis	16.35* (<0.01)	0.2* (<0.01)
	Femur	9.59* (0.02)	0.032* (<0.01)
	Tibia	20.28* (<0.01)	0.017* (<0.01)

Table 3. Percentages of covariance explained by the first axis obtained from each PLS analyses. Three series of PLS were performed: (i) with the Procrustes coordinates; (ii) with the size-free species averages; and (iii) with the size-free independent contrasts. S, scapula; H, humerus; R, radius; U, ulna; P, pelvis; F, femur; T, tibia.

		Procrustes coordinates	*Size-free species*	*Size-free contrasts*
Within limbs	S-H	74.96	70.1	53.27
	H-R	90.56	91.49	85.41
	H-U	88.85	91.83	90.93
	R-U	88.2	95.33	92.34
	P-F	66.27	68.63	37.55
	F-T	93.38	93.29	72.73
Between serial homologues	S-P	60	64.51	54.14
	H-F	82.6	81.86	80.13
	R-T	96.15	97.69	84.18
Between functional equivalents	U-T	94.46	97.57	88.83
	S-F	66.68	62.29	54.57
	H-T	95.77	95.09	80.86

Table 4. Bootstrap percentile and confidence intervals for the RV differences between cursors and non-cursors calculated using size-free independent contrasts. The 90% and 95% intervals are shown for the bootstrap percentile intervals (BPI) and bootstrap confidence intervals (BCI). Asterisks indicate significant cases.

		BPI 90%	BPI 95%	BCI 90%	BCI 95%
Within limbs	S-H	(-0.165, 0.324)	(-0.21, 0.368)	(-0.179, 0.313)	(-0.226, 0.36)
	H-R	(-0.068, 0.268)	(-0.101, 0.296)	(-0.028, 0.307)	(-0.06, 0.339)
	H-U	(-0.033, 0.243)	(-0.067, 0.268)	(0.023, 0.298)*	(-0.003, 0.325)
	R-U	(-0.027, 0.234)	(-0.055, 0.253)	(0.015, 0.275)*	(-0.009, 0.299)
	P-F	(-0.051, 0.405)	(-0.101, 0.442)	(0.031, 0.484)*	(-0.012, 0.527)
	F-T	(-0.065, 0.42)	(-0.107, 0.453)	(0.032, 0.516)*	(-0.014, 0.562)
Between serial homologues	S-P	(-0.118, 0.397)	(-0.171, 0.433)	(-0.121, 0.393)	(-0.17, 0.442)
	H-F	(-0.173, 0.141)	(-0.206, 0.166)	(-0.177, 0.136)	(-0.208, 0.166)
	R-T	(-0.016, 0.247)	(-0.038, 0.353)	(0.039, 0.373)*	(0.007, 0.405)*
Between functional equivalents	U-T	(-0.007, 0.328)	(-0.041, 0.355)	(0.04, 0.374)*	(0.007, 0.406)*
	S-F	(-0.031, 0.384)	(-0.072, 0.418)	(-0.012, 0.399)	(-0.052, 0.438)
	H-T	(-0.009, 0.391)	(-0.045, 0.428)	(0.069, 0.47)*	(0.03, 0.508)*

Figure 1. Graphic models showing the hypotheses of morphological integration in the appendicular skeleton investigated in this study. A, comparisons performed to investigate covariation (black lines) between anatomically connected bones (within-limbs) and between serially homologous and functional equivalent bones (between-limbs). B, hypothesis of functional integration postulated in this study: an increase in the strength of functional interactions within individuals, between both serial homologous (left) and functional equivalent bones (right), of specialized cursorial species (thick dark grey lines; blue lines in the online version). C, hypothesis of evolutionary integration postulated in this study: performance selection on individual function leading to an increase in the degree of covariation between serial homologous (left) and functional equivalent bones (right), which translates into a pattern of higher evolutionary integration in specialized taxa (thick light grey lines; orange lines in the online version). See the theoretical framework of Klingenberg (2008) and Klingenberg (2014) for the specific terminology. Abbreviations: S, scapula; H, humerus; R, radius; U, ulna; P, pelvis; F, femur; T, tibia.

Figure 2. Landmarks digitized to recover the shape of the appendicular bones. S, scapula; H, humerus; R, radius; U, ulna; P, pelvis; F, femur; T, tibia. See Table S2 for the anatomical criteria to locate the landmarks.

Figure 3. Phylogenetic tree topology used in this study for the order Carnivora.

Figure 4. Graphic models showing the RV coefficients obtained for the total sample. Each circle indicates a limb bone: S, scapula; H, humerus; R, radius; U, ulna; P, pelvis; F, femur; T, tibia. Grey boxes indicate the fore- and hind limbs separately. Each line

indicates the RV coefficient. RV values are shown and the line thickness is proportional to RV^2 (to more easily visualize the degree of covariation). RV coefficients were calculated from the Procrustes coordinates (A), size-free species averages (B), and size-free independent contrasts (C). Comparisons within-limb bones (left), between serial homologues (centre) and between functional equivalents (right) are shown separately.

Figure 5. Bivariate graphs with the first PLS axes obtained from the size-free species averages for the within-limb comparisons. A, scapula-humerus; B, humerus-radius; C, humerus-ulna; D, radius-ulna; E, pelvis-femur; F, femur-tibia. The bone models show the morphological changes associated with each axis. Symbols: grey squares, Ailuridae; black circles, Canidae; grey circles, Felidae; empty triangles, Hyaenidae; grey triangles, Mustelidae; empty circles, Procyonidae; empty squares, Ursidae. See Table 1 for species labels.

Figure 6. Bivariate graphs with the first PLS axes obtained from the size-free species averages for the between-limb comparisons. A, scapula-pelvis, B, humerus-femur; C, radius-tibia; D, ulna-tibia; E, scapula-femur; F, humerus-tibia. The bone models show the morphological changes associated with each axis. See Figure 5 for symbols and Table 1 for species labels.

Figure 7. Graphic models showing the RV coefficients obtained for cursors and non-cursors. Each circle indicates a limb bone: S, scapula; H, humerus; R, radius; U, ulna; P, pelvis; F, femur; T, tibia. Grey boxes indicate the fore- and hind limbs separately. Each line indicates a calculated RV coefficient. RV values are also shown and the line thickness is proportional to RV^2 for easier visualization. RV coefficients were

calculated from the size-free species averages for cursors (A) and non-cursors (B). RV coefficients were also calculated from the size-free independent contrasts for cursors (C) and non-cursors (D). Comparisons within-limb bones (left), between serial homologues (centre) and between functional equivalents (right) are shown separately. Statistically significant differences between RV coefficients with the 95 % (**) and 90% (*) for either bootstrap percentile or confidence intervals for cursors and non-cursors are indicated (for more information see Figure 8 and Table 4).

Figure 8. Frequency graphs obtained from the bootstrap analyses on RV differences for size-free species averages. Each graph shows the distribution of the differences between the RV coefficients for cursors and non-cursors (see main text for details) after 10,000 bootstrap resamples for each bone comparison. The *x*-axis indicates values of RV differences ($RV_{cursors} - RV_{non\text{-}cursors}$) and the *y*-axis indicates frequency. Areas beyond the 90% and 95% bootstrap percentile intervals are shown in dark grey and black, respectively. The position of the null value is indicated (dashed line). Tests for the within-limb comparisons: A, scapula-humerus; B, humerus-radius; C, humerus-ulna; D, radius-ulna; E, pelvis-femur; F, femur-tibia. Tests for the comparisons between serial homologues: G, scapula-pelvis; H, humerus-femur; I, radius-tibia. Tests for the comparisons between functional equivalents: J, ulna-tibia; K, scapula-femur; L, humerus-tibia.

SUPPORTING INFORMATION

Table S1. List of specimens analysed of the species included in this paper. Host institution and identity number (ID) are indicated. AMNH, American Museum of

Natural History (New York); NHM, Natural History Museum (London). * Indicates a specimen in which a bone was absent (S, scapula; P, pelvis; T, tibia).

Table S2. Detailed description of the anatomical position of each landmark used in this study.

Table S3. Results of the angular comparisons for the first PLS axis of each bone. The computed angle between each pair of PLS axes is shown. Asterisks denote significance at the 95% level. S, scapula; H, humerus; R, radius; U, ulna; P, pelvis; F, femur; T, tibia.

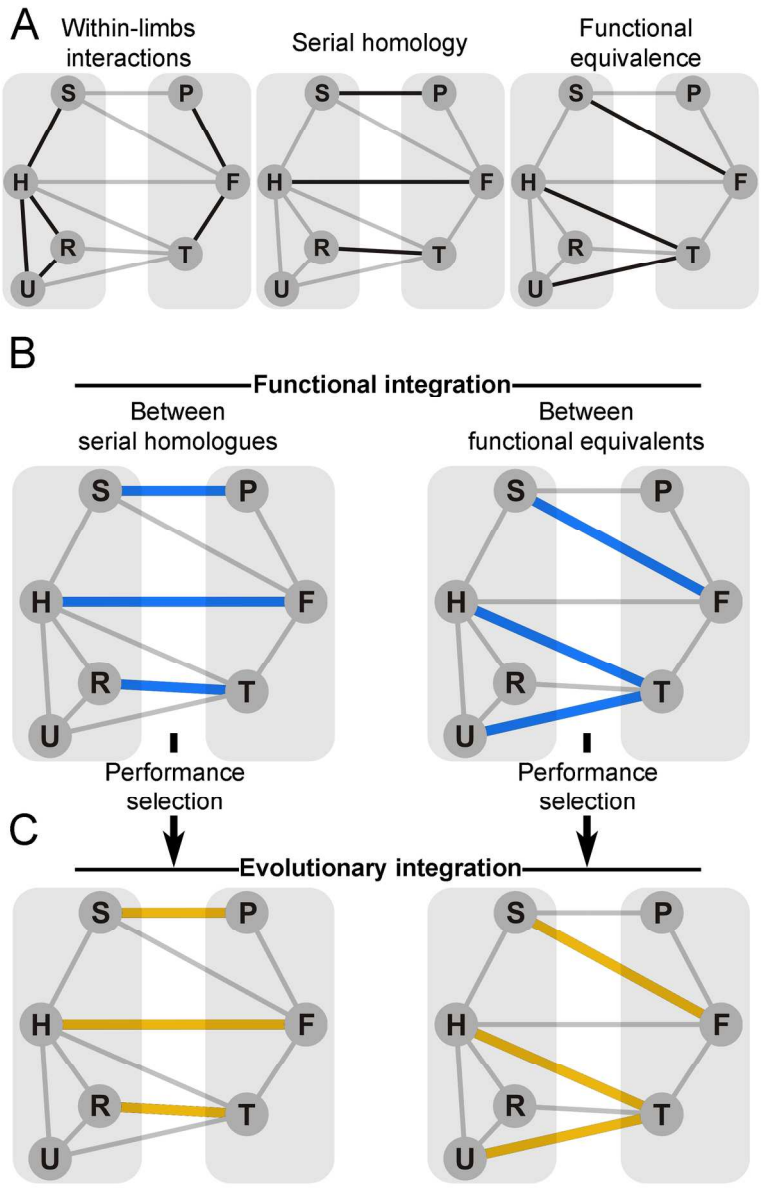

Figure 1. Graphic models showing the hypotheses of morphological integration in the appendicular skeleton investigated in this study. A, comparisons performed to investigate covariation (black lines) between anatomically connected bones (within-limbs) and between serially homologous and functional equivalent bones (between-limbs). B, hypothesis of functional integration postulated in this study: an increase in the strength of functional interactions within individuals, between both serial homologous (left) and functional equivalent bones (right), of specialized cursorial species (thick dark grey lines; blue lines in the online version). C, hypothesis of evolutionary integration postulated in this study: performance selection on individual function leading to an increase in the degree of covariation between serial homologous (left) and functional equivalent bones (right), which translates into a pattern of higher evolutionary integration in specialized taxa (thick light grey lines; orange lines in the online version). See the theoretical framework of Klingenberg (2008) and Klingenberg (2014) for the specific terminology. Abbreviations: S, scapula; H, humerus; R, radius; U, ulna; P, pelvis; F, femur; T, tibia.
137x213mm (300 x 300 DPI)

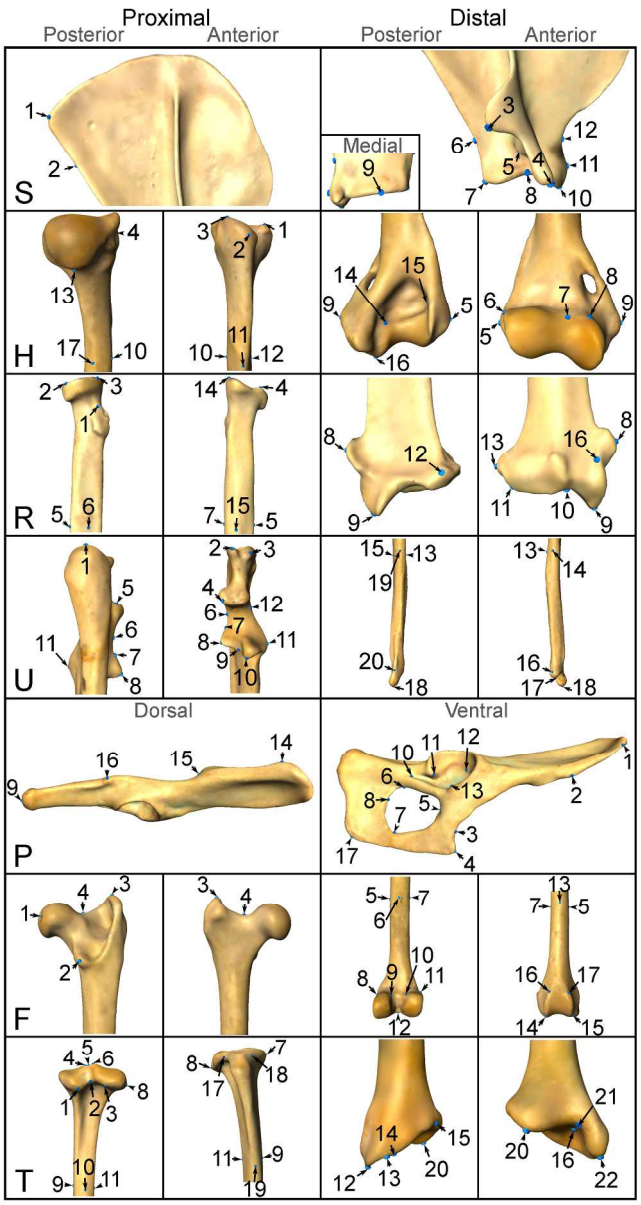

Figure 2. Landmarks digitized to recover the shape of the appendicular bones. S, scapula; H, humerus; R, radius; U, ulna; P, pelvis; F, femur; T, tibia. See Table S2 for the anatomical criteria to locate the landmarks.
166x314mm (300 x 300 DPI)

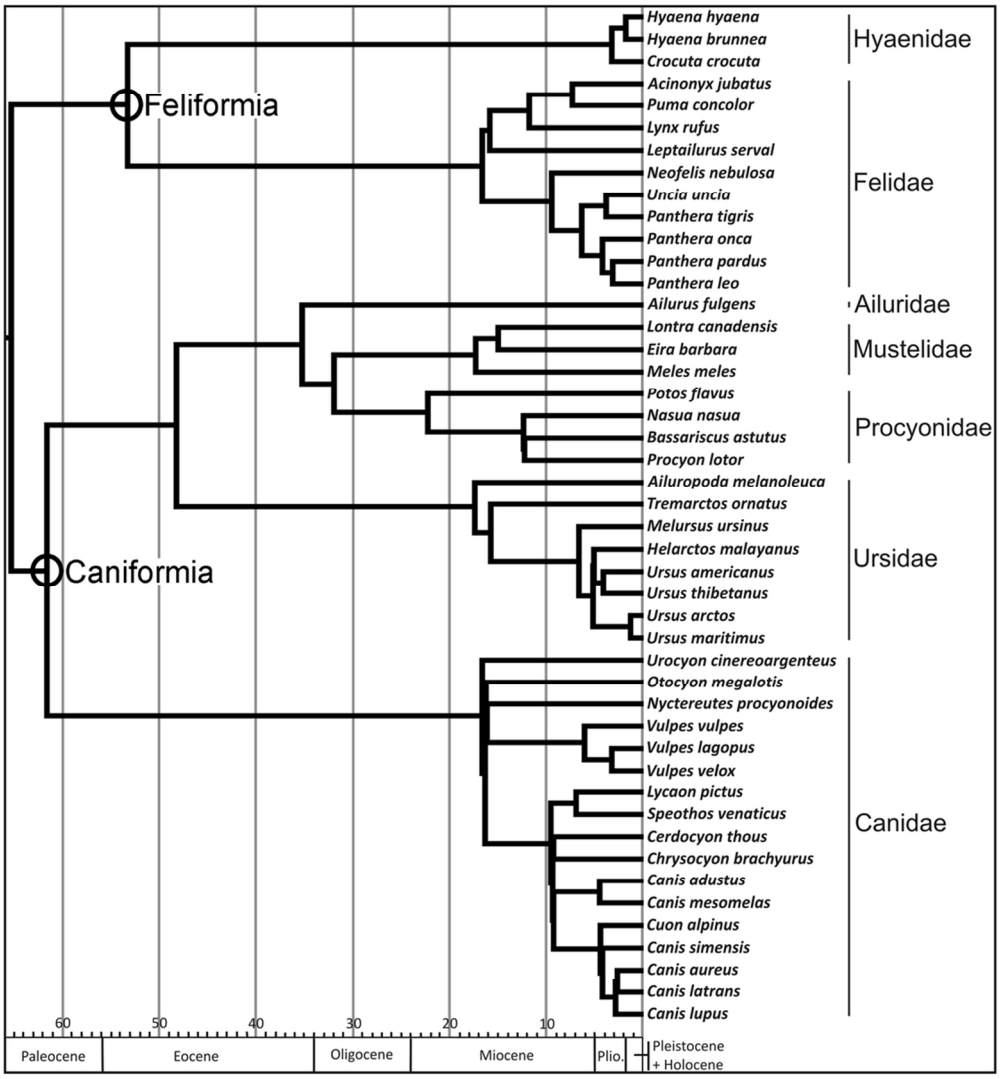

Figure 3. Phylogenetic tree topology used in this study for the order Carnivora.
95x103mm (300 x 300 DPI)

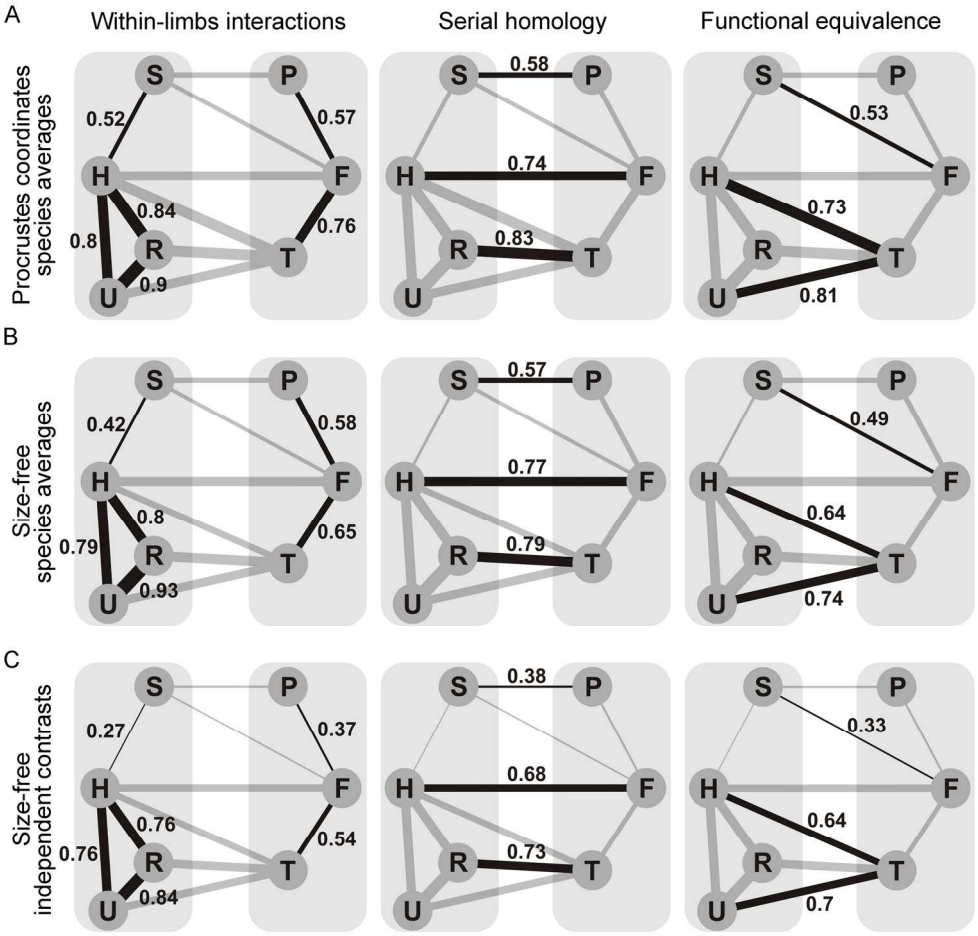

Figure 4. Graphic models showing the RV coefficients obtained for the total sample. Each circle indicates a limb bone: S, scapula; H, humerus; R, radius; U, ulna; P, pelvis; F, femur; T, tibia. Grey boxes indicate the fore- and hind limbs separately. Each line indicates the RV coefficient. RV values are shown and the line thickness is proportional to RV2 (to more easily visualize the degree of covariation). RV coefficients were calculated from the Procrustes coordinates (A), size-free species averages (B), and size-free independent contrasts (C). Comparisons within-limb bones (left), between serial homologues (centre) and between functional equivalents (right) are shown separately.
170x162mm (300 x 300 DPI)

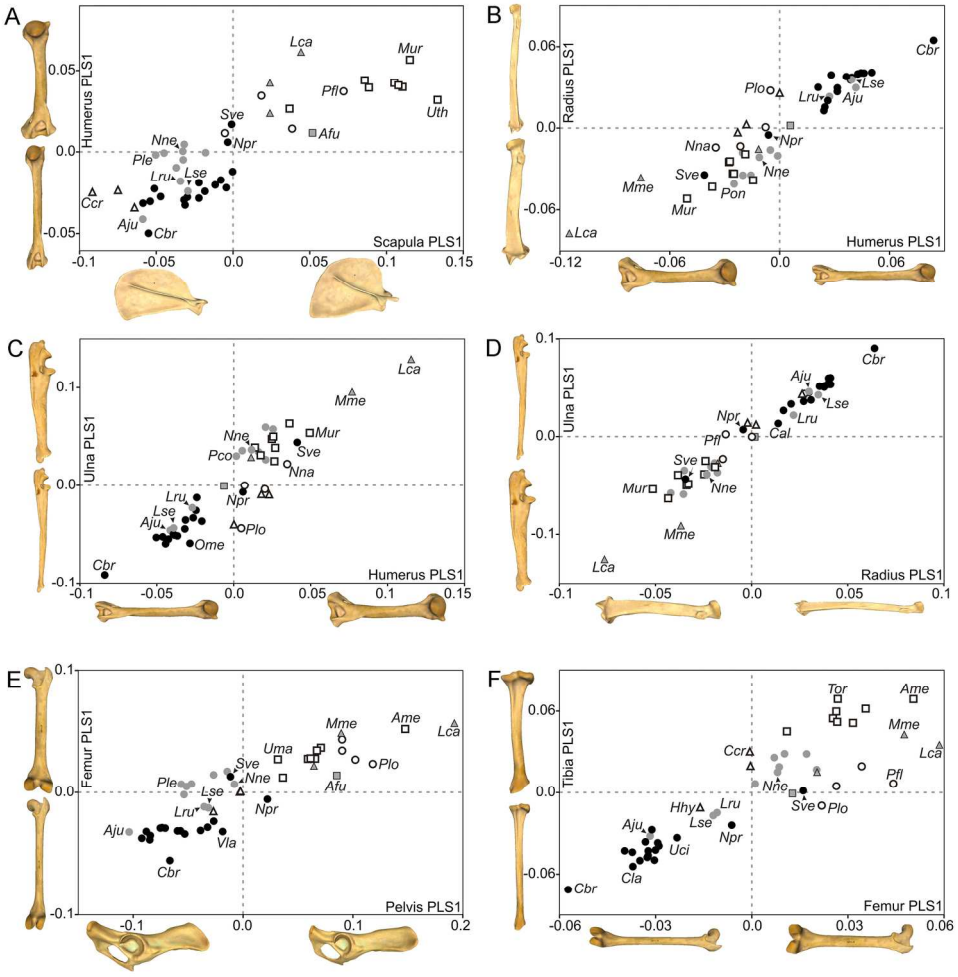

Figure 5. Bivariate graphs with the first PLS axes obtained from the size-free species averages for the within-limb comparisons. A, scapula-humerus; B, humerus-radius; C, humerus-ulna; D, radius-ulna; E, pelvis-femur; F, femur-tibia. The bone models show the morphological changes associated with each axis. Symbols: grey squares, Ailuridae; black circles, Canidae; grey circles, Felidae; empty triangles, Hyaenidae; grey triangles, Mustelidae; empty circles, Procyonidae; empty squares, Ursidae. See Table 1 for species labels.
181x183mm (300 x 300 DPI)

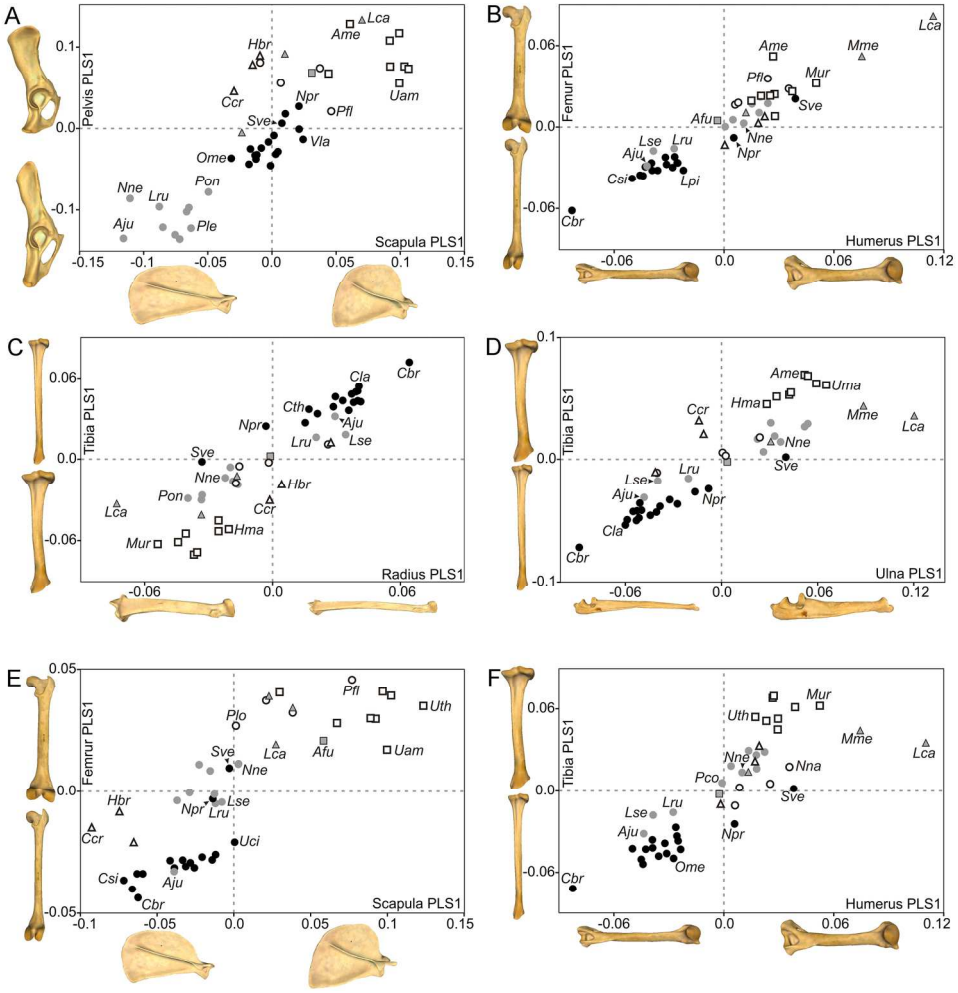

Figure 6. Bivariate graphs with the first PLS axes obtained from the size-free species averages for the between-limb comparisons. A, scapula-pelvis, B, humerus-femur; C, radius-tibia; D, ulna-tibia; E, scapula-femur; F, humerus-tibia. The bone models show the morphological changes associated with each axis. See Figure 5 for symbols and Table 1 for species labels.
182x184mm (300 x 300 DPI)

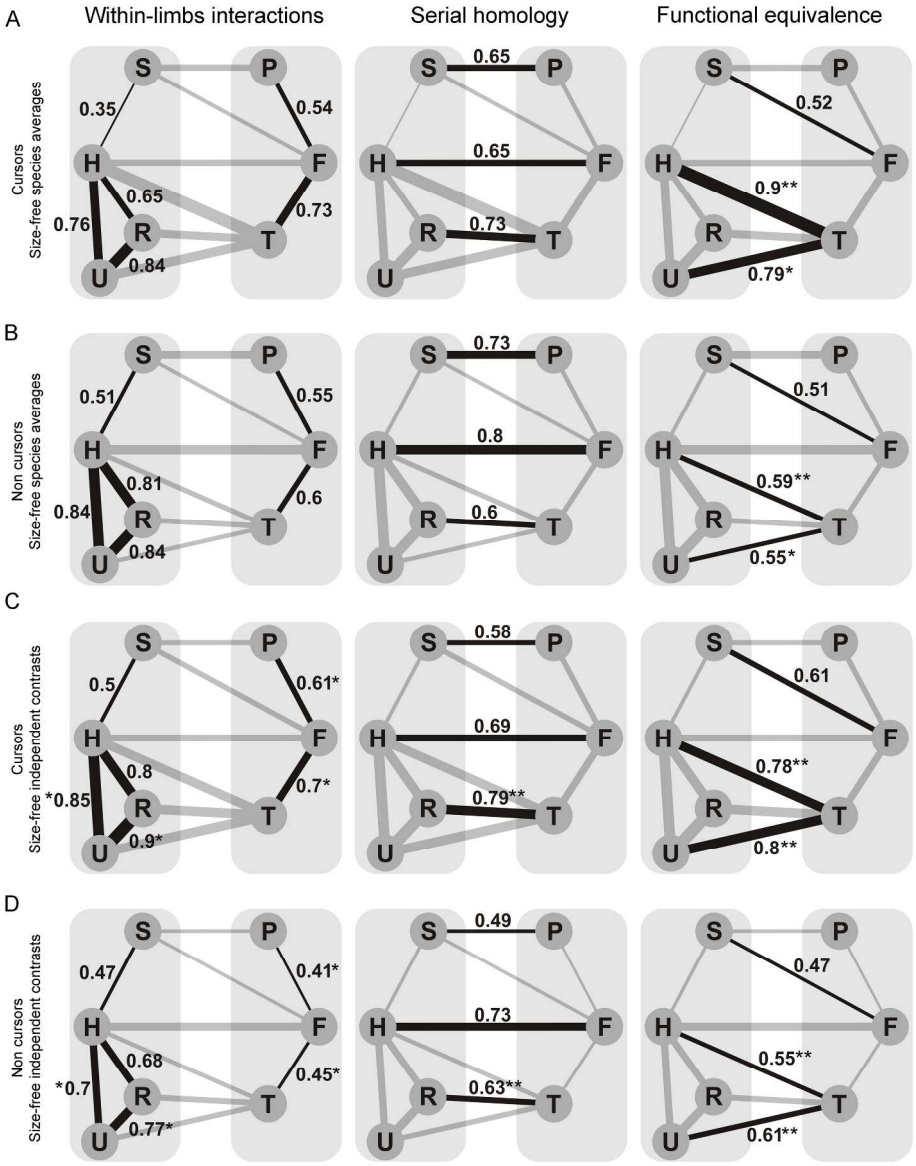

Figure 7. Graphic models showing the RV coefficients obtained for cursors and non-cursors. Each circle indicates a limb bone: S, scapula; H, humerus; R, radius; U, ulna; P, pelvis; F, femur; T, tibia. Grey boxes indicate the fore- and hind limbs separately. Each line indicates a calculated RV coefficient. RV values are also shown and the line thickness is proportional to RV2 for easier visualization. RV coefficients were calculated from the size-free species averages for cursors (A) and non-cursors (B). RV coefficients were also calculated from the size-free independent contrasts for cursors (C) and non-cursors (D). Comparisons within-limb bones (left), between serial homologues (centre) and between functional equivalents (right) are shown separately. Statistically significant differences between RV coefficients with the 95 % (**) and 90% (*) for either bootstrap percentile or confidence intervals for cursors and non-cursors are indicated (for more information see Figure 8 and Table 4).
229x293mm (300 x 300 DPI)

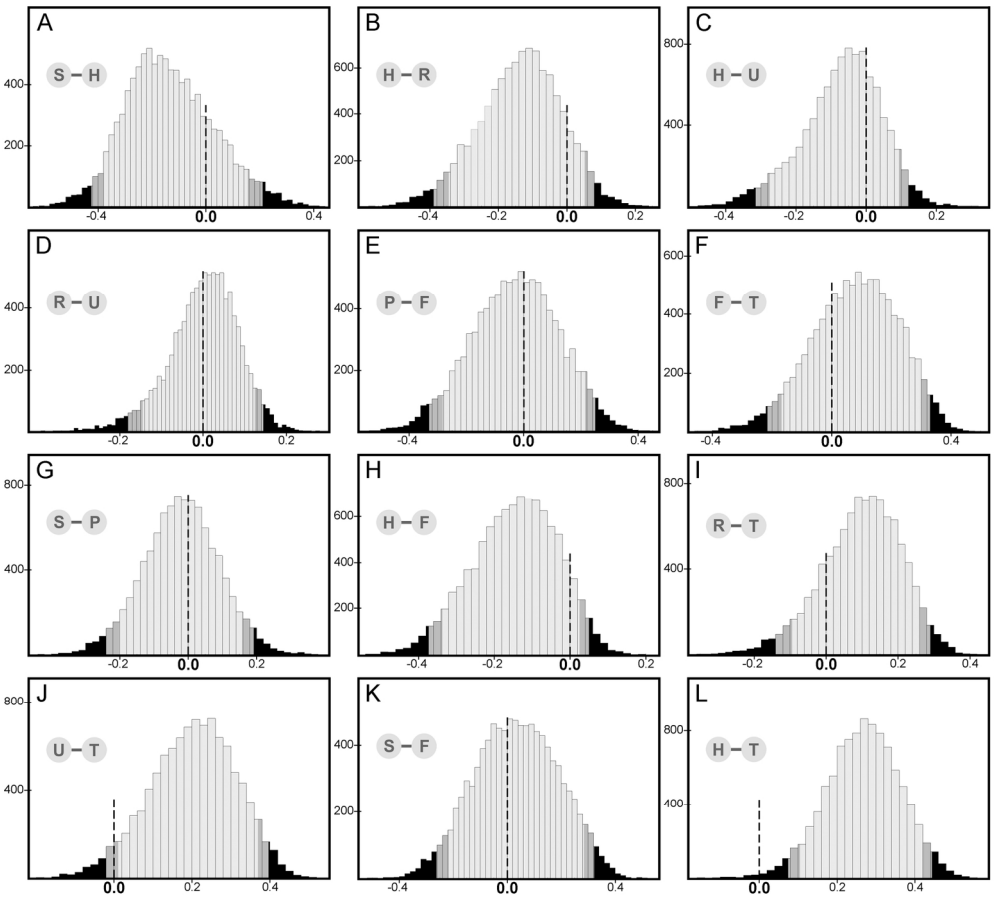

Figure 8. Frequency graphs obtained from the bootstrap analyses on RV differences for size-free species averages. Each graph shows the distribution of the differences between the RV coefficients for cursors and non-cursors (see main text for details) after 10,000 bootstrap resamples for each bone comparison. The x-axis indicates values of RV differences (RVcursors – RVnon-cursors) and the y-axis indicates frequency. Areas beyond the 90% and 95% bootstrap percentile intervals are shown in dark grey and black, respectively. The position of the null value is indicated (dashed line). Tests for the within-limb comparisons: A, scapula-humerus; B, humerus-radius; C, humerus-ulna; D, radius-ulna; E, pelvis-femur; F, femur-tibia. Tests for the comparisons between serial homologues: G, scapula-pelvis; H, humerus-femur; I, radius-tibia. Tests for the comparisons between functional equivalents: J, ulna-tibia; K, scapula-femur; L, humerus-tibia.
164x150mm (300 x 300 DPI)